Alkanethiols on Platinum: Multicomponent Self-Assembled Monolayers

Dmitri Y. Petrovykh,*,†,‡ Hiromi Kimura-Suda,§,|| Aric Opdahl,§,⊥ Lee J. Richter,§ Michael J. Tarlov,§ and Lloyd J. Whitman‡

Physics Department, University of Maryland, College Park, Maryland 20742, Naval Research Laboratory, Washington, D.C. 20375, and National Institute of Standards and Technology, Gaithersburg, Maryland 20899

Received April 7, 2005. In Final Form: November 23, 2005

We have studied the formation of self-assembled monolayers (SAMs) of *n*-alkanethiols on platinum thin films using X-ray photoelectron spectroscopy (XPS), reflection−absorption infrared spectroscopy (RAIRS), spectroscopic ellipsometry (SE), and contact angle (CA) measurements. Specifically, SAMs of 1-hexanethiol, 1-dodecanethiol, and 1-octadecanethiol were grown on polycrystalline Pt films, and the effects of Pt surface preparation, deposition conditions, and solvent treatments on the initial quality and stability of the monolayer in air were investigated. The SAMs prepared under ambient conditions on piranha-cleaned and UV/ozone-cleaned substrates were compared to monolayers formed on template-stripped Pt in an inert atmosphere. We found that alkanethiols deposited from 1 mM ethanolic solutions on piranha-cleaned Pt formed densely packed monolayers in which alkyl chains were oriented close to the surface normal. Stored in the laboratory ambient, these monolayers were unchanged over about 1 week but were largely oxidized in about 1 month. No evidence was found of molecules being weakly bound within the monolayer or having undergone C−S bond scission; however, three distinct sulfur states were observed for all samples in the XPS of the S 2p region. The lowest- and highest-binding-energy components are assigned to alkylthiolate and partially oxidized alkylthiolate species, respectively. The remaining S 2p component (approximately one-third of the sulfur layer), intermediate in binding energy between the other two components, is attributed to a chemisorbed species with a S binding configuration distinct from the majority alkylthiolate: for example, S bound to Pt bound to O, S with a different Pt coordination number, or S in an adsorbed disulfide.

1. Introduction

Recent developments in molecular electronic devices have stimulated interest in the formation of self-assembled monolayers (SAMs) of organic thiols on various metal surfaces. Because SAMs of alkanethiols on gold have been extensively characterized, most researchers have studied the electrical activity of molecules on gold substrates. However, both theoretical and practical considerations suggest that other metals should be considered for molecular electronics applications.[1] For example, a reduction of contact resistance by nearly 2 orders of magnitude has been achieved by interfacing SAMs with platinum vs gold electrodes.[2] From a fabrication point of view, gold is incompatible with silicon processing because of its high surface and bulk diffusivity, reactivity, and ability to form electronic defects.[3]

Several groups have begun to investigate the structure and stability of monolayers on metals other than Au, notably on Pd and Pt, which are considered to be good thiolate contact materials and to be compatible with the fabrication of silicon microelectronics. Two approaches have emerged for forming SAMs on Pt surfaces. The first approach attempts to avoid surface oxidation by minimizing exposure of samples to oxygen: deoxygenating solvents, handling samples in inert atmosphere, etc.[4−6] In the second approach, no explicit attempt is made to control the oxidation, and the deposition is carried out under more typical laboratory conditions—Pt cleaning by mechanical polishing[7] or in a piranha solution,[8] followed by alkanethiol deposition from an ethanolic solution. In this report, we use standard techniques to characterize the formation and longevity of alkanethiol SAMs on Pt under ambient conditions, in part to provide a direct comparison between SAMs on Au and those on Pt. Several samples prepared on Pt using oxygen-free deposition conditions are characterized as controls. A factor that influences the quality and stability of a thiol-based SAM is the bonding at the sulfur−substrate interface;[9] therefore, we specifically focus on the nature of the three distinct sulfur states observed in SAMs on Pt by X-ray photoelectron spectroscopy (XPS). Although a number of systematic structure and stability studies have been carried out for SAMs on Au,[8−11] to our knowledge, this is the first such study for SAMs on Pt.

2. Materials and Methods

2.1. Materials. Commercially available 1-hexanethiol, 1-dodecanethiol, and 1-octadecanethiol were used without further purifica-

* To whom correspondence should be addressed. Dmitri Y. Petrovykh, Code 6177, Naval Research Laboratory, Washington, D.C. 20375-5342. E-mail: dmitri.petrovykh@nrl.navy.mil.

† University of Maryland.

‡ Naval Research Laboratory.

§ National Institute of Standards and Technology.

|| Current address: PerkinElmer Japan Co., Ltd., Yokohama, Japan.

⊥ Current address: Department of Chemistry, University of Wisconsin, La Crosse, WI 54601.

(1) Chen, Y.; Ohlberg, D. A. A.; Li, X. M.; Stewart, D. R.; Williams, R. S.; Jeppesen, J. O.; Nielsen, K. A.; Stoddart, J. F.; Olynick, D. L.; Anderson, E. *Appl. Phys. Lett.* **2003**, *82*, 1610−1612.

(2) Beebe, J. M.; Engelkes, V. B.; Miller, L. L.; Frisbie, C. D. *J. Am. Chem. Soc.* **2002**, *124*, 11268−11269.

(3) Graff, K. *Metal Impurities in Silicon Device Fabrication*; Springer-Verlag: Berlin, 1995; Vol. 24.

(4) Vilar, M. R.; Bouali, Y.; Kitakatsu, N.; Lang, P.; Michalitsch, R.; Garnier, F.; Dubot, P. *Thin Solid Films* **1998**, *329*, 236−240.

(5) Li, Z. Y.; Chang, S. C.; Williams, R. S. *Langmuir* **2003**, *19*, 6744−6749.

(6) Brito, R.; Tremont, R.; Feliciano, O.; Cabrera, C. R. *J. Electroanal. Chem.* **2003**, *540*, 53−59.

(7) Laiho, T.; Leiro, J. A.; Lukkari, J. *Appl. Surf. Sci.* **2003**, *212*, 525−529.

(8) Schlenoff, J. B.; Li, M.; Ly, H. *J. Am. Chem. Soc.* **1995**, *117*, 12528−12536.

(9) Laibinis, P. E.; Whitesides, G. M.; Allara, D. L.; Tao, Y. T.; Parikh, A. N.; Nuzzo, R. G. *J. Am. Chem. Soc.* **1991**, *113*, 7152−7167.

(10) Rieley, H.; Kendall, G. K.; Zemicael, F. W.; Smith, T. L.; Yang, S. H. *Langmuir* **1998**, *14*, 5147−5153.

(11) Schoenfisch, M. H.; Pemberton, J. E. *J. Am. Chem. Soc.* **1998**, *120*, 4502−4513.

10.1021/la050928a CCC: $33.50
Published on Web 02/17/2006

tion. Hereafter, an abbreviated notation for these alkanethiols, C6SH, C12SH, and C18SH, respectively, is used in the text, and C6, C12, and C18 labels are used to indicate the number of alkyl chain carbons in the figures. Ethanol (95%, hereafter EtOH) and dichloromethane (HPLC grade, hereafter CH_2Cl_2) were used as received (except where noted otherwise) for the preparation of 1 mM solutions of alkanethiols and for rinsing or soaking samples after monolayer deposition.

2.2. Platinum Film Cleaning and SAM Deposition. Diced fragments from platinum-coated silicon wafers were used as substrates (200 nm of Pt sputter-deposited over a 30 nm Ti adhesion layer). The Pt films exhibited an rms roughness of 1.7 nm over an area of 1 μm^2 as measured by atomic force microscopy (AFM). Prior to SAM deposition, the diced substrates (≤ 2 cm^2) were cleaned by immersion in a "piranha" solution consisting of 70% H_2SO_4 and 30% H_2O_2 (30% H_2O_2 in water). (***Caution****: This solution must be handled with care; it is extremely oxidizing, reacts violently with organics, and should only be stored in loosely tightened containers to avoid pressure buildup*.) Piranha-cleaned Pt will hereafter be denoted p-Pt. After being cleaned, each p-Pt substrate was immediately and thoroughly rinsed with high-resistivity water ($\sim$18.2 MΩ·cm) that had been treated to remove organic and biological impurities. To deposit monolayers, the cleaned substrates were submerged in 1 mM solutions of alkanethiols in EtOH for 20 h at room temperature. For comparison purposes, SAMs were prepared from identical solutions on piranha-cleaned Au substrates (200 nm of Au evaporated over a 20 nm Cr adhesion layer on silicon), hereafter p-Au. After deposition, each sample was rinsed thoroughly with EtOH and then dried in a stream of dry nitrogen. To measure the stability of the deposited monolayers, the samples were exposed to ambient laboratory air for periods ranging from 1 h to 55 days.

To examine solvent effects, control samples were soaked in CH_2Cl_2 overnight after the above standard EtOH deposition or deposited from 1 mM solutions of alkanethiols in CH_2Cl_2. In another series of controls, substrates were cleaned using a commercial UV/ozone cleaner (hereafter UVO-Pt), rather than in piranha solution. UVO cleaning was performed for about 20 min in ozone generated in situ from atmospheric oxygen by a low-pressure mercury quartz lamp (185 and 254 nm UV range, $\sim$25 mW/cm^2 power).

2.3. Template-Stripped Platinum Films and Oxygen-Free SAM Deposition. Template-stripped Pt (TS-Pt) films were prepared following the protocol of Blackstock et al.[12] Briefly, a 220 nm Pt film was sputter-deposited on a piranha-cleaned ultraflat Si(100) wafer. The Pt film was then removed (stripped) from this template by using an adhesive-covered Si substrate. The TS-Pt films exhibited an rms roughness of 0.7 nm over an area of 1 μm^2 as measured by AFM. The stripping was performed inside an inert-atmosphere glovebox to limit oxidation of the TS-Pt substrate. Monolayers were then deposited in the glovebox, from 1 mM solutions in solvents that were distilled under nitrogen and calcium hydride. Hereafter, these conditions will be referred to as "oxygen-free" deposition.

2.4. XPS Measurements. XPS measurements were performed using a commercial system equipped with a monochromatic Al Kα source, a hemispherical electron energy analyzer (58° angle between monochromator and analyzer), and a magnetic electron lens. The nominal XPS spot size and analyzer field of view were ≤ 1 mm^2. The binding energies (BEs) are reported with 0.1 eV precision based on a two-point BE scale calibration to the BEs of Au $4f_{7/2}$ (84.0 eV) and Au $4f_{5/2}$ (335.2 eV) measured in each run for Au films cleaned by Ar ion sputtering.[13,14] In each run, we also measured BEs of 71.1 eV for Pt $4f_{7/2}$ and 314.6 eV for Pt $4d_{5/2}$ from freshly sputter-cleaned Pt films, in agreement with the accepted values of 71.12 and 314.61 eV, respectively.[14] For the thin organic monolayers in this study, charge compensation was not necessary and was not applied.

We present data acquired in normal-emission angle-integrated scans of the Pt 4f, Pt 4d, S 2p, C 1s, and O 1s regions (15−20 eV windows with 0.1 eV spacing, 20 eV pass energy, 0.36 eV analyzer resolution). Spectra of the S 2p regions were accumulated for 30−45 min, to obtain a signal-to-noise ratio adequate for resolving the multiple components. Typically, spectra were acquired from three separate spots on each sample, primarily to test the monolayer uniformity. The corresponding calculated coverage values varied by no more than 10% for each of the samples. The reference Pt and Au spectra used to calibrate the attenuation of the XPS signals were measured from substrates cleaned in situ by Ar ion sputtering until C 1s and O 1s signals were no longer detectable.

2.5. XPS Peak Fitting. The peaks in the elemental core-level spectra were fit using commercial XPS analysis software.[15] A convolution of Lorentzian and Gaussian line shapes was used to fit the individual peaks.[16] A linear combination of Shirley and linear functions was used to model the background, with the corresponding coefficients fit simultaneously with the peaks. The only exception was for fits in the O 1s region, where additional polynomial terms were added to model the nonlinear background caused by the proximity of the Pt $4d_{3/2}$ peak. Multiple-component fitting in the C 1s and S 2p regions, always started from the lowest BE component and its full-width at half-maximum (fwhm), was used to constrain the fwhm's for the higher-BE components.[16] In each case, the minimum number of components that produced unstructured fit residuals was chosen.

2.6. RAIRS Measurements. Reflection−absorption infrared spectroscopy (RAIRS) was performed using a commercial Fourier transform spectrometer equipped with a wire-grid polarizer (p-polarized) and a variable-angle reflectance accessory (reflectance angle 75°). RAIRS spectra were collected from 4000 to 900 cm^{-1} using a cryogenic mercury cadmium telluride (MCT) detector (1024 scans at 2 cm^{-1} resolution). The spectra were referenced to a bare Pt substrate, cleaned by the respective procedure. The RAIRS measurements were performed on freshly prepared samples prior to XPS characterization.

2.7. SE Measurements. Spectroscopic ellipsometry (SE) was performed using a commercial multichannel instrument with a rotating compensator and 190−1000 nm wavelength working range. The Pt substrates for SE measurements were $\sim$1 cm^2 chips diced from a single Pt-covered wafer and cleaned by piranha or UVO treatment. The analysis was performed with vendor-supplied software.

2.8. CA Measurements. Contact angle (CA) measurements were performed at room temperature and ambient relative humidity using high-resistivity water as the probing liquid. Sessile contact angles were measured with $\sim$5 μL of water dropped onto the surfaces from a syringe needle and recorded immediately after the drop. Measurements from three different spots were averaged for each sample.

3. Experimental Results

3.1. Effects of Solvents and Substrate Cleaning on Monolayer Deposition. We used XPS as the primary method for quantitative analysis of the structure and stability of alkanethiol monolayers. XPS has been widely used to characterize SAMs, e.g., on Au,[9−11,17−26] Ag,[8,9,11,23,25,27,28] Cu,[8,9,25,29−31] Ni,[32] Pd,[33] and Pt.[5−8,34,35] The XPS spectrum of the S 2p region is particularly useful for characterizing alkanethiol SAMs, because the position and intensity of the S 2p peaks can be used to identify and

(12) Blackstock, J. J.; Li, Z. Y.; Freeman, M. R.; Stewart, D. R. *Surf. Sci.* **2003**, *546*, 87−96.

(13) Seah, M. P.; Gilmore, L. S.; Beamson, G. *Surf. Interface Anal.* **1998**, *26*, 642−649.

(14) Powell, C. J. *Appl. Surf. Sci.* **1995**, *89*, 141−149.

(15) Hesse, R.; Chasse, T.; Szargan, R. *Fresenius J. Anal. Chem.* **1999**, *365*, 48−54.

(16) The total fwhm is the sum of Gaussian and Lorentzian contributions. The Lorentzian fwhm was 0.1 eV for C 1s and O 1s and 0.25 eV for S 2p. For C 1s components C2 and C3, the total fwhm was fixed to that of C1 (1.2−1.3 eV). For S 2p components, we used a spin−orbit intensity ratio of 0.5 and an energy splitting of 1.2 eV.; the total fwhm was 0.98 eV for S1 and S2, 1.48 eV for S3.

(17) Castner, D. G.; Hinds, K.; Grainger, D. W. *Langmuir* **1996**, *12*, 5083−5086.

(18) Ishida, T.; Hara, M.; Kojima, I.; Tsuneda, S.; Nishida, N.; Sasabe, H.; Knoll, W. *Langmuir* **1998**, *14*, 2092−2096.

(19) Heister, K.; Frey, S.; Golzhauser, A.; Ulman, A.; Zharnikov, M. *J. Phys. Chem. B* **1999**, *103*, 11098−11104.

(20) Heister, K.; Allara, D. L.; Bahnck, K.; Frey, S.; Zharnikov, M.; Grunze, M. *Langmuir* **1999**, *15*, 5440−5443.

(21) Yan, C.; Golzhauser, A.; Grunze, M.; Woll, C. *Langmuir* **1999**, *15*, 2414−2419.

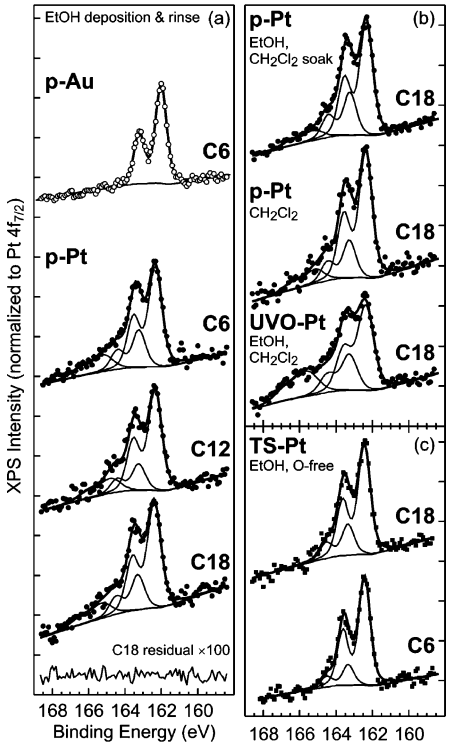

Figure 1. XPS of the S 2p region for as-deposited alkanethiol SAMs on Pt. (a) Deposition from 1 mM solution in EtOH, rinse in EtOH: C6SH on p-Au (○); C6SH, C12SH, and C18SH on p-Pt (●). (b) C18SH on p-Pt: deposition from 1 mM solution in EtOH, overnight soak in CH_2Cl_2 (top); deposition from 1mM solution in CH_2Cl_2 (middle); deposition from 1 mM solution in EtOH on UVO-Pt substrate, overnight soak in CH_2Cl_2 (bottom). (c) C18SH and C6SH deposition on TS-Pt in an inert-atmosphere glovebox from 1 mM solutions in deoxygenated EtOH. Open and solid symbols = data, thick lines = total fits, thin lines = peak components and backgrounds. The residual for the C18SH/p-Pt fit is shown at the bottom of panel a.

quantify various monolayer components (chemisorbed, physisorbed, oxidized). Figure 1a shows S 2p spectra for monolayers deposited on p-Pt from 1 mM ethanolic solutions of C6SH, C12SH, and C18SH (solid symbols) as well as a reference spectrum for C6SH deposited on p-Au (open symbols, top of Figure 1a). The spectra are shown normalized to the intensity of the respective substrate signals (Pt $4f_{7/2}$ or Au $4f_{7/2}$); the C6SH/p-Au spectrum is also scaled by the ratio of Scofield factors for Au $4f_{7/2}$ and Pt $4f_{7/2}$.[36,37]

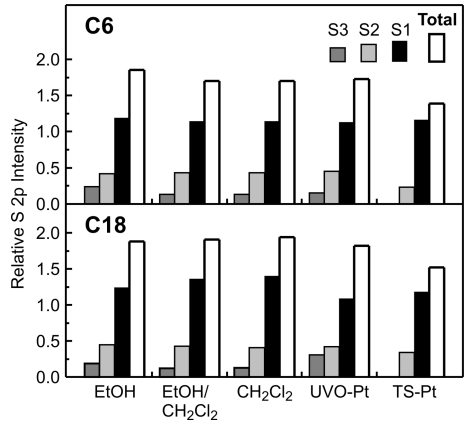

Figure 2. XPS S 2p components for alkanethiol SAMs deposited on Pt under different conditions. Intensity is normalized to the S 2p peak for the C6SH/p-Au SAM in Figure 1.

The C6SH/p-Au reference spectrum in Figure 1a is clearly consistent with a *single* S 2p doublet; the BE of 162.0 and fwhm of 0.84 eV[16] are in excellent agreement with previous studies of alkylthiolates on Au.[10,17,18,20−24,38,39] In contrast, all of the S 2p spectra for SAMs on Pt in Figure 1a are distinctly multicomponent, with at least three components required to obtain unstructured residuals.[40] Hereafter, these three components will be referred to as S1, S2, and S3 in order of increasing BE. The BE of the S1 component is 162.3 eV for C6SH and C12SH and 162.4 eV for C18SH.[16] The S2-to-S1 relative BE shift is 0.85−0.95 eV in unrestricted fits and hereafter is fixed at 0.9 eV for consistency. The S3-to-S1 relative BE shifts are between 2.4 and 3.1 eV.

Control experiments, results of which are presented in Figure 1b and c, were performed to explore the effect of deposition conditions on initial SAM quality and corresponding S 2p components. In SAMs on Au, the most common assignment of S 2p components with BEs of around 163.5 eV (i.e., S2 in our case) is to unbound thiols physisorbed or trapped in the monolayer. Existence of a similar unbound component has also been proposed for SAMs on Pd[33] and Pt.[5] To investigate this possibility, we carried out two types of control experiments: deposition from 1 mM ethanolic solutions followed by an overnight soak in CH_2Cl_2 and deposition from 1 mM solutions in CH_2Cl_2. An overnight soak in CH_2Cl_2, a good solvent for alkanethiols, is expected to remove any weakly bound alkanethiols left after a standard deposition from EtOH. Similarly, deposition from CH_2Cl_2, although potentially slower, should significantly suppress any weakly bound components. Figure 1a and b shows little, if any, change in the S2 and S3 components following the CH_2Cl_2 treatments. Only the monolayers grown in an inert atmosphere on TS-Pt substrates were noticeably different: the S3 component was eliminated and S2 significantly reduced (Figure 1c). These trends can be more clearly seen in Figure 2, which shows relative

(22) Kawasaki, M.; Sato, T.; Tanaka, T.; Takao, K. *Langmuir* **2000**, *16*, 1719−1728.
(23) Heister, K.; Zharnikov, M.; Grunze, M.; Johansson, L. S. O. *J. Phys. Chem. B* **2001**, *105*, 4058−4061.
(24) Yang, Y. W.; Fan, L. J. *Langmuir* **2002**, *18*, 1157−1164.
(25) Laibinis, P. E.; Bain, C. D.; Whitesides, G. M. *J. Phys. Chem.* **1991**, *95*, 7017−7021.
(26) Hansen, H. S.; Tougaard, S.; Biebuyck, H. *J. Electron Spectrosc. Relat. Phenom.* **1992**, *58*, 141−158.
(27) Himmelhaus, M.; Gauss, I.; Buck, M.; Eisert, F.; Woll, C.; Grunze, M. *J. Electron Spectrosc. Relat. Phenom.* **1998**, *92*, 139−149.
(28) Ohgi, T.; Fujita, D.; Deng, W.; Dong, Z. C.; Nejoh, H. *Surf. Sci.* **2001**, *493*, 453−459.
(29) Laibinis, P. E.; Whitesides, G. M. *J. Am. Chem. Soc.* **1992**, *114*, 9022−9028.
(30) Ron, H.; Cohen, H.; Matlis, S.; Rappaport, M.; Rubinstein, I. *J. Phys. Chem. B* **1998**, *102*, 9861−9869.
(31) Sung, M. M.; Sung, K.; Kim, C. G.; Lee, S. S.; Kim, Y. *J. Phys. Chem. B* **2000**, *104*, 2273−2277.
(32) Mekhalif, Z.; Laffineur, F.; Couturier, N.; Delhalle, J. *Langmuir* **2003**, *19*, 637−645.
(33) Love, J. C.; Wolfe, D. B.; Haasch, R.; Chabinyc, M. L.; Paul, K. E.; Whitesides, G. M.; Nuzzo, R. G. *J. Am. Chem. Soc.* **2003**, *125*, 2597−2609.
(34) Brito, R.; Rodriguez, V. A.; Figueroa, J.; Cabrera, C. R. *J. Electroanal. Chem.* **2002**, *520*, 47−52.
(35) Long, Y. T.; Herrwerth, S.; Eck, W.; Grunze, M. *Phys. Chem. Chem. Phys.* **2002**, *4*, 522−526.
(36) Scofield, J. H. *J. Electron Spectrosc. Relat. Phenom.* **1976**, *8*, 129−137.
(37) Normalizing elemental XPS signals by the corresponding Scofield factors (ref 36) is a standard way to correct for element-dependent photoelectric cross sections, the major factor that determines element-specific XPS intensities. This normalization ignores any spatial distribution of the elements, but provides a practical way to compare elemental intensities, as such Scofield-adjusted intensity ratios often appear in quantitative XPS analysis models (see Appendix).
(38) Vericat, C.; Vela, M. E.; Andreasen, G.; Salvarezza, R. C.; Vazquez, L.; Martin-Gago, J. A. *Langmuir* **2001**, *17*, 4919−4924.
(39) Zerulla, D.; Chasse, T. *Langmuir* **1999**, *15*, 5285−5294.
(40) The Tougaard model with parameters established for SAMs/Au (ref 26) predicts intensities of inelastic backgrounds to be much lower than the observed high-BE shoulders of S 2p peaks. The asymmetric S 2p peak shapes thus correspond to multiple S 2p components.

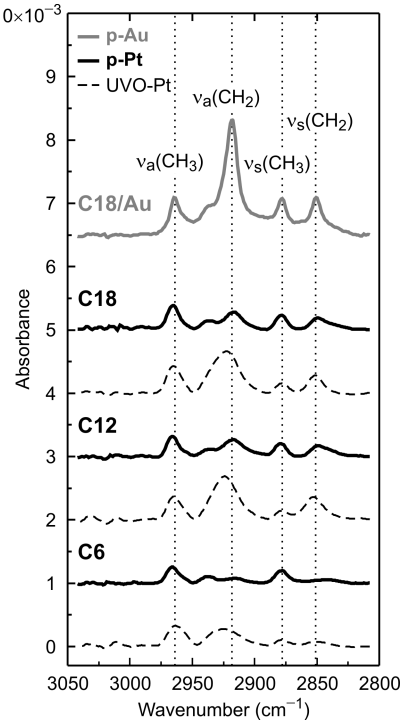

Figure 3. RAIRS spectra of C−H region for alkanethiol SAMs prepared on Pt substrates cleaned by two different methods. Deposition is from 1 mM ethanolic solutions followed by rinse in EtOH.

Table 1. Vibrational Line Positions for C18SH Monolayers on Au and Pt

	C18SH/p-Au		C18SH/p-Pt		C18SH/UVO-Pt	
peak assignment[a]	ν (cm^{-1})	fwhm (cm^{-1})	ν (cm^{-1})	fwhm (cm^{-1})	ν (cm^{-1})	fwhm (cm^{-1})
$\nu_s(CH_2)$ sym str	2853	13	2850	11	2851	15
$\nu_s(CH_3)$ sym str	2879	10	2878	8	2878	11
$\nu_a(CH_2)$ asy str	2918	12	2917	17	2923	24
$\nu_s(CH_3)$ FR sym str	2936	20	2937	12	2936	10
$\nu_a(CH_3)$ op asy str	2958	8	na[b]		na[b]	
$\nu_a(CH_3)$ ip asy str	2964	8	2965	10	2965	13

[a] The following abbreviations are used: str, stretch; sym, symmetric; asym, antisymmetric; ip, inplane; op, out of plane; FR, Fermi resonance component. [b] Not observed.

intensities of the total S 2p signal and the individual components for C6SH and C18SH monolayers prepared using all of the methods shown in Figure 1. The relative intensities correspond to peak areas in Figure 1 normalized to the area of the S 2p peak for the reference C6SH/p-Au SAM. Notably, both the S1 and S2 components are essentially independent of deposition conditions in both absolute and relative terms. The corresponding monolayer coverages are quantified in section 4.2, and the nature of the S 2p components is further discussed in section 4.4.

Figure 3 shows RAIRS spectra for freshly deposited C6SH, C12SH, and C18SH monolayers using Pt substrates cleaned by two different methods: p-Pt and UVO-Pt. Table 1 lists the peak parameters for the C18SH films.[41] The RAIRS data for monolayers on TS-Pt substrates are presented in the Supporting Information (Figure SI1, Table SI1). The RAIRS peak assignments follow ref 42. The spectra for SAMs on UVO-Pt exhibit wide and unresolved peaks, indicating relatively disordered

(41) The spectra were analyzed by nonlinear least-squares fitting to multiple Lorentzian lines, except in the case of the UVO-Pt substrate, in which a Gaussian line shape was required.

(42) Parikh, A. N.; Allara, D. L. *J. Chem. Phys.* **1992**, *96*, 927−945.

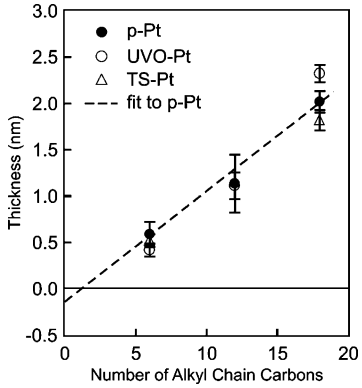

Figure 4. Comparison of ellipsometric thickness of alkanethiol monolayers on variously cleaned Pt substrates. Linear fit to the data for p-Pt: $t_{SE} = (0.12 \pm 0.01) \cdot n_C - (0.14 \pm 0.2)$ (Pearson's r factor = 0.978).

monolayers. In fact, they are very similar to those reported for SAMs on platinum oxide.[5] By contrast, monolayers deposited from EtOH on p-Pt have peak frequencies and widths similar to those of SAMs on p-Au (Table 1) and SAMs on plasma-cleaned Pt.[5] The intensities of the CH_2 features, relative to the CH_3 features, are lower for our p-Pt samples than for p-Au and plasma-cleaned Pt,[5] indicating orientation of the alkyl chains closer to the surface normal (see section 4.1).

We characterized the optical thickness of freshly deposited SAMs by SE for all three substrates (p-Pt, UVO-Pt, and TS-Pt). The optical constants of Pt films are expected to vary with Pt deposition and cleaning conditions; therefore, it is crucial to develop a proper dielectric model for the metal substrate. The SE data for a series of samples, namely, a substrate freshly cleaned by the respective procedure and C6SH, C12SH, and C18SH SAMs, were simultaneously fit to a three-phase optical model consisting of a common Pt substrate, an organic layer of variable thickness, and air. The index of refraction ($\hat{n} = n + ik$) of the organic layer was held at 1.50, consistent with earlier treatments of alkanethiol SAMs on Au.[43] Optical thickness, t_{SE}, as a function of the number of alkyl chain carbons, n_C, is shown in Figure 4. The error bars reflect multiple measurements (2 or 3) for multiple sample series (2 or 3). The optical thicknesses of the monolayers are similar for all surface treatments.

We used water CA measurements as a standard characterization method for hydrophobic methyl-terminated SAMs. For as-deposited monolayers the sessile contact angles were 91° (C6SH), 101° (C12SH), and 104° (C18SH) on p-Pt and 88° (C6SH), 99° (C12SH), and 101° (C18SH) on UVO-Pt. Overall, the CA values are about 10° lower than those reported for SAMs on Au, Ag, and Cu.[9] Our values are also about 5° lower than previous results reported for SAMs/Pt.[5] The trend of increasing CA with alkyl chain length agrees with results for SAMs on Au, Ag, Cu,[9] and Pt.[5] Smaller CA values for oxidized UVO-Pt are also in agreement with previous results.[5]

3.2. SAM Stability in Air. The photoemission spectra of the S 2p region in Figure 5 show the changes in oxidation and coverage of SAMs/p-Pt exposed to air. We show the data for C6SH for the first few days (top three curves in Figure 5) because these thinner monolayers result in lower XPS signal attenuation and, thus, higher signal-to-noise ratios for S2 and S3 components. Over the long term, the thickest SAMs are typically the most stable; thus, we show data for C18SH for the bottom two curves in Figure 5.

(43) Shi, J.; Hong, B.; Parikh, A. N.; Collins, R. W.; Allara, D. L. *Chem. Phys. Lett.* **1995**, *246*, 90−94.

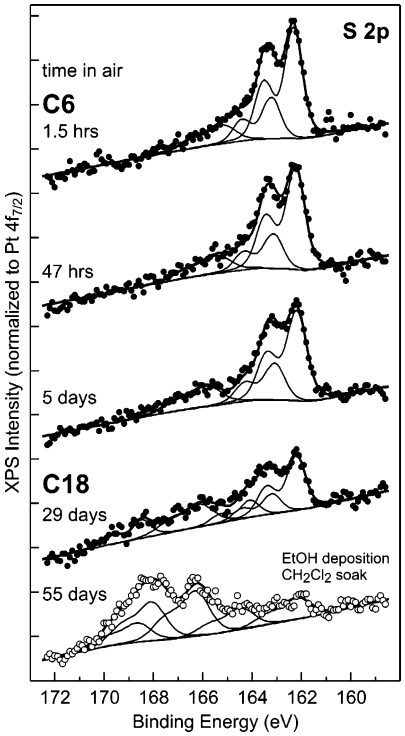

Figure 5. XPS of the S 2p region for SAMs/p-Pt exposed to ambient air. Exposure time and alkyl chain length as shown. Deposition and rinse in EtOH. Bottom spectrum (○) is for a C18SH SAM soaked overnight in CH_2Cl_2 before exposure to air. Open and solid circles = data, thick lines = total fits, thin lines = peak components and backgrounds.

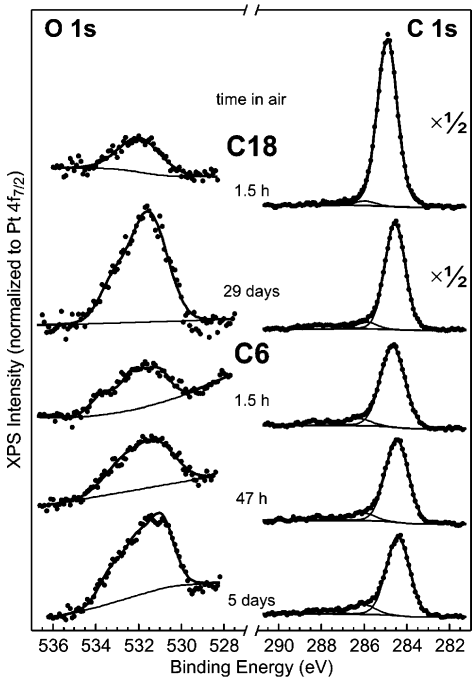

Figure 6. XPS of O 1s and C 1s regions for SAMs/p-Pt exposed to air. Deposition and rinse in EtOH (top to bottom): C18SH SAMs exposed to air for 1.5 h and 29 days (C 1s spectra are shown scaled by $^1/_2$); C6SH SAMs exposed to air for 1.5 h, 47 h, and 5 days. Solid circles = raw data, thick lines = total fits, thin lines = peak components and backgrounds.

For the first 5 days, the main change in the S 2p spectra is a gradual shift of the S3 component to higher BE: the average BE of the S3 component changes from 165.0 to 165.5 to 165.8 eV (Figure 5). This BE shift is consistent with partial oxidation of 10−15% of the sulfur headgroups. At the same time, the intensities of all three components remain nearly constant, indicating that desorption or redistribution of molecules in the monolayer does not occur for the first 5 days. In contrast, after 29 days, about one-half of the original intensity of S1−S3 components has been lost for the C18SH monolayer, and additional high-BE components have appeared.

The bottom spectrum in Figure 5 corresponds to a C18SH monolayer deposited using the EtOH/CH_2Cl_2 procedure. After 55 days in air, it shows the greatest oxidation of the samples we examined. By comparison, in a recent study of SAMs on Pd, a similarly severe degree of oxidation was observed for a hexadecanethiol monolayer after only 5 days in air (cf. Figure 6c in ref 33); thus, it appears that monolayers on Pt are significantly more stable against exposure to air than those on Pd.

Complementary information about the oxidation of SAMs under ambient conditions is provided by photoemission spectra of the O 1s and C 1s regions (Figure 6). For all samples, the intensity in the O 1s region is spread over about 4 eV. Given the typical fwhm of about 1.5 eV for O 1s in organic materials, this indicates at least three different chemical states for oxygen. The broad O 1s envelope and nonstoichiometric composition of surface oxides do not allow us to make corresponding assignments of the observed O 1s components with any certainty. The total O 1s intensity increases monotonically with exposure to air, as expected. The lowest O 1s signal in the p-Pt series was observed for an as-deposited C18SH monolayer (top spectrum in Figure 6).[44] The C 1s spectra in all cases are dominated by the main peak (C1) with BE between 284.5 and 284.9 eV that corresponds to the hydrocarbon chains. At least two additional components (C2 and C3) had to be added to the fits to produce unstructured residuals.[16,45]

To quantitatively compare the oxidation data from S 2p and O 1s regions (Figures 5 and 6), we used Scofield-adjusted S 2p and O 1s intensity ratios to the Pt $4f_{7/2}$ substrate peak,[36,37] as shown for C18SH monolayers on p-Pt in Figure 7 (Table SI2). There is little change in the S 2p components over the first 5 days of exposure to air (Figures 5 and 7). Between 5 and 29 days in air, the intensity of the S3 component increases, whereas the total S 2p and the S1 intensities decrease (Figure 7). These trends are consistent with increased oxidation of alkylthiolate S groups and associated desorption of alkylthiols. Another notable trend is that the intensity of the S2 component does not increase with air exposure; thus, unlike the S3 component, the S2 component is not associated with a final product of oxidation. The stability and oxidation trends are similar for all of the alkyl chain lengths that we have examined (Table SI2, Supporting Information).

The CA, RAIRS, and SE techniques are sensitive to the ordering of alkyl chains, but only minor changes were observed after a few days in air. The CA values changed by <5% for the C6SH

(44) The oxygen-free deposition on TS-Pt substrates resulted in the lowest overall O 1s signals in our study. For C6SH/TS-Pt, the Scofield-adjusted intensity ratios (same units as in Table SI2) are 227 for the C2 and C3 components, 220 for O 1s, and 101 for S2. The total intensity of the oxidized C components is equal to the total O signal; thus, the data are consistent with essentially no PtO_x on the surface while S2 is still present.

(45) Each of the alkanethiol molecules contains two chemically distinct carbon atoms: one bound to the sulfur headgroup and one in the methyl group. The former is likely to have a BE higher than the alkyl carbons of the main C1 peak. The C2/C1 intensity ratios in fits to our data (Figure 6), however, are about one-half of what would be expected for ideal SAMs of respective thicknesses. An additional component of the appropriate intensity and BE shift of <1 eV can be added without sacrificing the quality of the fits to account for the headgroup-bound carbons. The C2 and C3 components then must be interpreted as due to adventitious and/or solvent molecules. In the literature, assignment of C 1s components with BE shifts of 1.2−1.6 eV (C2) and 2.7−3.6 eV (C3) varies, e.g., refs 6 and 27.

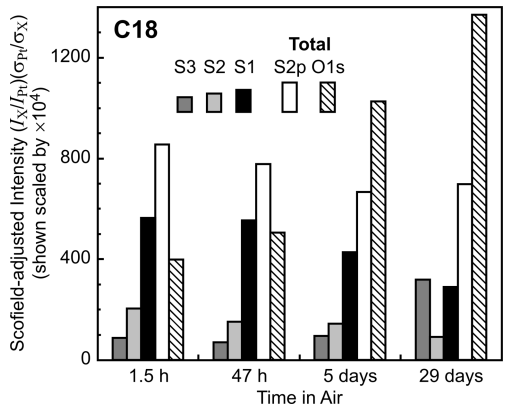

Figure 7. Evolution of O 1s and S 2p intensities for C18SH SAMs/p-Pt exposed to air. Component labels and intensities are the same as in Figures 5 and 6. Note that the initial total O signal is less than the total S signal.

and C18SH monolayers (EtOH/CH_2Cl_2 deposition) after 7 days in air. In RAIRS spectra taken after 7 days in air, the peak shapes and intensities remained essentially unchanged, except for a small shift of $\nu_a(CH_2)$ from 2917 cm^{-1} to higher wavenumbers. SE showed a slight 0.1 ± 0.1 nm increase in film thickness over the first 8 days, possibly due to adsorption of adventitious hydrocarbons. These results are consistent with the retention of nearly the full monolayer, indicating that the structure changes induced by air exposure over the first few days are limited to the S−metal interface.

4. Discussion

4.1. Monolayer Thickness, Stoichiometry, and Molecular Orientation. The IR-active CH_2 stretch frequencies are sensitive to the local intermolecular interactions and thus serve as the primary indicator of chain order.[46,47] For C18SH on p-Pt, the observed $\nu_a(CH_2)$ frequency (2917 cm^{-1}) is characteristic of an ordered, all-trans chain and is essentially the same as those reported in a previous study of SAMs on plasma-cleaned Pt,[5] indicating a similarly high degree of crystalline order. For all monolayers on p-Pt the $\nu_s(CH_2)$ and $\nu_a(CH_2)$ features are strongly suppressed compared to the CH_3 features (Figure 3). The transition dipole moments of the CH_2 modes are perpendicular to the all-trans chain, whereas both the $\nu_s(CH_3)$ and $\nu_a(CH_3)$ modes have transition dipole moment projections along the chain axis. The suppressed intensity of the CH_2 stretches indicates an orientation almost perpendicular to the surface normal.

To quantitatively determine the monolayer orientation, we performed a detailed analysis of the RAIRS data for C18SH on p-Pt films.[42] Determination of the tilt angle for the presumed all-trans methylene chain is very sensitive to the preparation of the bulk reference spectrum.[48] We therefore used the C18SH/Au spectrum and the known orientation of the monolayers on Au as a reference. Assuming that the C18SH/Au tilt angle lies between 20° and 30°, the tilt angle for C18SH/p-Pt lies between 6° and 16°. This is consistent with the qualitative observation that the C18SH/p-Pt spectrum is very similar to that reported for C18SH on Ag, where the tilt angle was determined to be 12°.[9] There is very little difference between the intensities of the CH_2 peaks in the RAIRS spectra of C12SH and C18SH, implying that the tilt angle must decrease with chain length.

(46) MacPhail, R. A.; Strauss, H. L.; Snyder, R. G.; Elliger, C. A. *J. Phys. Chem.* **1984**, *88*, 334−341.
(47) Snyder, R. G.; Strauss, H. L.; Elliger, C. A. *J. Phys. Chem.* **1982**, *86*, 5145−5150.
(48) Arnold, R.; Terfort, A.; Woll, C. *Langmuir* **2001**, *17*, 4980−4989.

Table 2. Evolution of Monolayer Thickness and Stoichiometry with Exposure to Air

sample	thickness[a] (nm)	calculated elemental attenuation and ratio C*[b]	S*[c]	C*/S*	experimental C/S ratio[d]
1.5 h					
C6SH	0.80	5.47	0.81	6.8	7.5
C12SH	1.60	9.84	0.66	14.9	16.1
C18SH	2.40	13.3	0.53	25.1	24.8
47 h					
C6SH	1.01	5.35	0.77	6.9	7.7
C18SH	2.23	13.6	0.56	24.3	26
5 days					
C6SH	0.78	5.48	0.82	6.7	7.5
C12SH	1.50	9.96	0.68	14.6	12.5
C18SH	2.28	13.5	0.55	24.6	25.8
29 days					
C12SH	1.30	10.2	0.71	14.4	12.5
C18SH	1.97	14.0	0.60	23.4	21.7

[a] Thickness t_{XPS} calculated from the attenuation of the Pt 4f and 4d photoelectrons, EAL(Pt $4f_{7/2}$) = 4.01 nm and EAL(Pt $4d_{5/2}$) = 3.48 nm.[25] Values calculated from Pt 4f and 4d attenuation differed by <3%; their average is reported. [b] Predicted carbon signal C* is calculated as a sum of contributions from n_C = 6, 12, or 18 layers (as applicable) attenuated by the thickness of the overlaying layers (assuming a thickness of t_{XPS}/n_C for each carbon layer), EAL(C 1s) = 3.54 nm.[25] [c] Predicted sulfur signal S* calculated assuming attenuation by the total monolayer thickness, EAL(S 2p) = 3.82 nm.[25] [d] Experimental Scofield-adjusted C 1s/S 2p intensity ratio.[36,37]

Quantitative analysis of the XPS intensities provides insight into both the film thickness and the stoichiometry. Reported in Table 2 is the monolayer photoelectron thickness, t_{XPS}, calculated from the attenuation of Pt $4f_{7/2}$ and Pt $4d_{5/2}$ substrate peaks (see Appendix A1).[25] These photoelectron thicknesses for as-deposited monolayers are linear as a function of the number of carbon atoms n_C [$t_{XPS} = (0.13 \cdot n_C)$ nm] and are very close to the extended lengths of the respective molecules [$t = (0.127 \cdot n_C)$ nm expected for upright chains]. The absolute values of photoelectron thicknesses support the nearly upright alkyl chain orientation established from the quantitative analysis of the RAIRS data. This is further corroborated by the linear regression to the SE data (Figure 4). Notably, our XPS and SE thickness measurements are consistent with absence of an oxide layer on p-Pt, as both yield offsets close to zero, in contrast with previously reported ellipsometric results for SAMs on Pt[5] and Pd.[33]

The stoichiometry (C/S ratio) can be estimated from the C and S signals, properly accounting for their respective attenuation due to their position in the film (see Appendix A1). The S signal is attenuated by the full monolayer thickness (S* in Table 2). The C contributions from each atomic layer are added from top to bottom with increasing attenuation (C* in Table 2). These predicted C*/S* ratios are compared in Table 2 to measured C/S ratios; the good agreement between the two columns leads us to two conclusions. First, the *n*-alkanethiol molecules are oriented with sulfur groups bound to the Pt surface and hydrocarbon tails extended away from the S/Pt interface. Second, little or no C−S bond scission occurs when alkanethiols self-assemble on Pt surfaces. In fact, the measured C/S ratio remains above the stoichiometric value even for monolayers either deposited or soaked in CH_2Cl_2—the treatments that should at least partially remove alkyl chains produced by such hypothetical C−S bond scission.

4.2. Coverage. In Table 3, the intensities of the S 2p components and the total S coverage are quantified for SAMs/Pt deposited under the different conditions presented in Figure 1. The relative intensities in Table 3 correspond to peak areas in

Table 3. S 2p Components and Sulfur Coverage for SAMs/Pt

sample description	S 2p components[a] S3	S2	S1	total	total sulfur coverage Au reference[b] 10^{14} atoms/cm^2
p-Pt, EtOH[c]					
C6SH	0.24	0.42	1.19	1.85	5.9
C12SH	0.22	0.32	1.17	1.71	5.5
C18SH	0.19	0.45	1.24	1.88	6.0
p-Pt, EtOH/CH_2Cl_2[d]					
C6SH	0.13	0.43	1.14	1.70	5.5
C18SH	0.12	0.43	1.36	1.91	6.1
p-Pt, CH_2Cl_2[e]					
C6SH	0.13	0.43	1.14	1.70	5.5
C18SH	0.13	0.41	1.40	1.94	6.2
UVO-Pt, EtOH/CH_2Cl_2[f]					
C6SH	0.15	0.45	1.13	1.73	5.5
C12SH	0.21	0.42	1.19	1.82	5.8
C18SH	0.31	0.42	1.09	1.82	5.8
TS-Pt, EtOH, Ar[g]					
C6SH	0	0.23	1.16	1.39	4.5
C18SH	0	0.34	1.18	1.52	4.9

[a] Intensities of S 2p components correspond to those in Figure 1 and are reported relative to the S 2p peak for C6SH/p-Au sample, i.e., as Scofield-adjusted[36,37] S 2p/Pt $4f_{7/2}$ intensity ratios divided by 0.0455. For most samples, intensity variation within a sample was <5%; a few outliers showed up to 10% variability. [b] Absolute coverages are calculated using a clean Au absolute reference and an empirical sensitivity factor to account for the difference between Pt and Au substrates (see Appendix A2 and Supporting Information for details). [c] Deposition from 1 mM solution in EtOH, rinse in EtOH. [d] Deposition from 1 mM solution in EtOH, overnight soak in CH_2Cl_2. [e] Deposition from 1 mM solution in CH_2Cl_2, rinse in CH_2Cl_2. [f] Deposition from 1 mM solution in EtOH, overnight soak in CH_2Cl_2, UVO-Pt substrate. [g] Deposition in inert-atmosphere glovebox from 1 mM solution in deoxygenated EtOH, rinse in EtOH, TS-Pt substrate.

Figure 1 normalized by the S 2p peak for the C6SH/p-Au SAM. Quantitatively, these Scofield-adjusted S 2p/Pt $4f_{7/2}$ intensity ratios[36,37] are converted into absolute S coverages in the following way: For the reference C6SH/p-Au SAM, we have an absolute calibration that gives a coverage of 4.5×10^{14} cm^{-2} (Appendix A2). We then use an empirical sensitivity factor established from measurements of clean Au and Pt substrates to obtain absolute coverages from S 2p/Pt $4f_{7/2}$ intensity ratios and the absolute Au reference. The resulting coverage values are reported in Table 3; for details and extensive discussion of this quantification approach see Appendix A2 and the Supporting Information. The estimated experimental uncertainty of the coverage values in Table 3 is about 10%; potential sources of systematic uncertainties are difficult to quantify, but some are discussed in the Supporting Information. With the exception of the TS-Pt substrates, the coverage of freshly deposited films is about 5.8×10^{14} cm^{-2}. The high areal density (relative to thiols on Au) is consistent with the near-normal chain orientation. SE measurements do not estimate monolayer thickness and coverage independently, but if the density and index of refraction of high-density polyethylene (HDPE) are used to estimate the coverage of C18SH/p-Pt, the result is $(4-5) \times 10^{14}$ cm^{-2}. For comparison, previous radiolabeling measurements showed 15% higher coverage for SAMs on Pt vs Au, which, assuming negligible roughness, is 5.3×10^{14} cm^{-2} for SAMs on Pt.[8] A recent scanning tunneling microscopy (STM) study reported a high-coverage phase for alkanethiols on Pt(111) with a $(\sqrt{3} \times \sqrt{3})R30°$ structure that corresponds to a 5.1×10^{14} cm^{-2} coverage.[49] These literature coverage values are thus somewhere between the XPS-determined coverages for SAMs on p-Pt and TS-Pt.

4.3. Platinum Oxide. As a practical matter, it is important to note that submonolayer amounts of platinum oxides readily form on clean Pt surfaces: experiments in ultrahigh vacuum (UHV) show that molecular oxygen dissociates and chemisorbs on Pt even at cryogenic temperatures.[50−53] Therefore, the presence of such surface platinum oxides can be assumed in most cases (especially when exposure to ambient is involved), and the interaction of thiols with these oxides will likely play a role in SAM formation and stability.

XPS potentially has the sensitivity to detect a submonolayer of platinum oxide through examination of the Pt 4f or O 1s peaks. Unfortunately, the Pt 4f peaks produce a highly asymmetric inelastic background, which makes it difficult to reliably detect a small platinum oxide component shifted by only about 0.9 eV.[54] For example, we observe no consistent difference between the shape of the Pt 4f spectra for freshly sputtered Pt substrates and those oxidized by UVO treatment. Therefore, the absence of platinum oxide components in the Pt 4f region, that the authors of refs 5 and 55 interpret as evidence of oxide-free Pt surfaces, in fact, only rules out the presence of (several) monolayers but not of a submonolayer of platinum oxide. The total O 1s signal gives an upper limit to the amount of platinum oxide as one-half that of the S for as-deposited samples on p-Pt substrates (Figure 7). The association of some of the oxygen with oxidized components of C and S prevents a more accurate estimate for platinum oxide.

We have evidence that UVO cleaning oxidizes Pt. For UVO-Pt samples, the O 1s signal was consistently about twice as high as that for samples on p-Pt or TS-Pt. RAIRS and SE indirectly corroborate the oxidation of UVO-Pt substrates. The RAIRS data for monolayers on UVO-Pt in Figure 3 show broader peaks similar to those reported for SAMs on platinum oxide.[5] The substrate dielectric constants, determined from the SE multisample analysis, were significantly different for the UVO-Pt and p-Pt surfaces (Figure SI2, Supporting Information). If we assume that the p-Pt is "clean" and the UVO-Pt has a thin oxide, then the bare UVO-Pt substrate data can be well fit to a three-phase optical model (substrate, oxide, air) with an oxide thickness of 0.53 ± 0.03 nm and a constant $\hat{n} = 1.76 \pm 0.02 + (0.34 \pm 0.11)$i.[56,57] The oxide film index of refraction is very similar to that obtained by SE (350−700 nm) for the hydrous form of PtO_2 formed by anodic oxidation in H_2SO_4 ($\hat{n} \approx 1.70 + 0.15$i).[58]

Can alkanethiols reduce these oxides on p-Pt and UVO-Pt? A positive claim of a complete reduction of thermal platinum oxide by alkanethiols has been reported on the basis of electrochemical measurements.[59] However, alkanethiol deposition

(49) Yang, Y.-C.; Yen, Y.-P.; Yang, L.-Y. O.; Yau, S.-L.; Itaya, K. *Langmuir* **2004**, *20*, 10030−10037.
(50) Puglia, C.; Nilsson, A.; Hernnas, B.; Karis, O.; Bennich, P.; Martensson, N. *Surf. Sci.* **1995**, *342*, 119−133.
(51) Stipe, B. C.; Rezaei, M. A.; Ho, W. *J. Chem. Phys.* **1997**, *107*, 6443−6447.
(52) Saliba, N.; Tsai, Y. L.; Panja, C.; Koel, B. E. *Surf. Sci.* **1999**, *419*, 79−88.
(53) Gambardella, P.; Sljivancanin, Z.; Hammer, B.; Blanc, M.; Kuhnke, K.; Kern, K. *Phys. Rev. Lett.* **2001**, *8705*.
(54) Bancroft, G. M.; Adams, I.; Coatsworth, L. L.; Bennewitz, C. D.; Brown, J. D.; Westwood, W. D. *Anal. Chem.* **1975**, *47*, 586−588.
(55) Li, Z. Y.; Beck, P.; Ohlberg, D. A. A.; Stewart, D. R.; Williams, R. S. *Surf. Sci.* **2003**, *529*, 410−418.
(56) Uncertainties are one standard deviation averaged over five measurement series.
(57) The unique extraction of dielectric constants from ultrathin (≤10 nm) films is problematic as the film thickness and index become correlated. The correlation coefficient between thickness and the real part of the index (n) was ~0.93. However, the estimated parameters are considered unique, as the statistical estimate of the fit uncertainties on thickness and n, accounting for the off-diagonal elements of the error matrix, are comparable to (~50% smaller than) the reported uncertainties based on multiple data sets.
(58) Gottesfeld, S.; Maia, G.; Floriano, J. B.; Tremiliosi, G.; Ticianelli, E. A.; Gonzalez, E. R. *J. Electrochem. Soc.* **1991**, *138*, 3219−3224.

Table 4. M−S and M−O Bond Strengths for fcc Metals

metal	Au	Ag	Cu	Ni	Pt
M−S[a]	418	217	276	344	234[b]
M−O[a]	222	220	269	382	392

[a] Values in kJ/mol from Bond Strengths in Diatomic Molecules. In *Handbook of Chemistry and Physics*; CRC Press: Boca Raton, FL, 2003; pp 9-52−9-64. These bond strengths, often known as the bond dissociation energies, are defined as the standard enthalpy change of the dissociation reaction as determined at 298 K. [b] Value converted from 56 kcal/mol give in Table 3 of ref 60, which defines bond strength as "the cohesive energy per metal−sulfur bond".

can suppress platinum oxide reduction features in voltammograms by either removing the oxide or by adsorbing on top of the oxide; thus, a submonolayer amount of residual oxide could remain undetected electrochemically. In general, the stability of thiolates against oxidation and the ability of thiols to reduce metal oxides depend in part on the respective metal−oxygen (M−O) and metal−sulfur (M−S) bond energies (Table 4). Of the metals in Table 4, only for Au is the M−S bond stronger than M−O, and the bond strength hierarchy is reversed for Pt. It is practically impossible to prepare oxide-free surfaces of Ag, Cu, or Ni in an ambient environment, and thus, SAM formation for all three of these metals is affected by the presence of such residual oxides.[27,30−32] Overall, the comparison with other fcc metals and the bond strength arguments suggest that a complete reduction of surface platinum oxides by alkanethiols is unlikely.

4.4. Assignment of S 2p Components in XPS Data. The interpretation of the three S 2p components in the XPS data (Figures 1 and 5) is key to understanding the structure of SAMs on Pt. Such assignments for SAMs on metals other than Au are at best tentative in the literature, and often are in conflict with each other. Here, we attempt to combine our high-resolution spectra of the S 2p region with results previously obtained for alkanethiol SAMs on a broad range of metal substrates (Au, Ag, Cu, Ni, Pd, and Pt) in order to provide the most consistent interpretation. We first briefly discuss the S3 component, and then we focus on the S1 (162.3 eV BE) and S2 (163.2 eV BE) components.

S3 Component. The assignment of the S3 (BE about 165 eV) and higher-BE components (e.g., see the bottom two spectra in Figure 5) is rather straightforward, as they are generally believed to result from increasingly higher oxidation states of sulfur, with S 2p doublets at 165 eV assigned as S^{4+} and those above 167 eV as sulfates.[61] Two trends in our data support this assignment. First, with exposure to air, the intensity of the S3 component increases (both in absolute value and relative to the S1), whereas the S1 intensity decreases (Figures 5 and 7), indicating that the primary mechanism of forming the S3 component in the ambient is oxidation of the S1 component. Second, the S3 component gradually shifts to higher BE with exposure to air, e.g., the average BE of the S3 component for C6SH monolayers increases from 165.0 to 165.8 eV (Figure 5). This shift indicates slow conversion of S from thiolates into higher oxidation states. A related observation concerning all of the high-BE S 2p components is that the oxidation of thiol groups in SAMs on Pt appears to proceed in a multistep fashion, i.e., through a variety of states with increasing oxidation, rather than directly into well-defined sulfates as reported for Cu.[29]

The *initial* amount of the S3 component in the monolayers correlates with Pt oxidation. In our study, the UVO-Pt substrates are the most oxidized (section 4.3), and the S3 component is correspondingly the highest for SAMs on UVO-Pt (Figure 1 and Table 3). This observation is in agreement with the data for SAMs on plasma-oxidized Pt, which showed considerable intensity above 164 eV BE.[5] Conversely, for SAMs prepared on TS-Pt under oxygen-free conditions, the S3 component is undetectable (Figure 1c). The correlation between the S3 and surface oxidation leads us to conclude that the initial oxidation of thiols is mediated or facilitated by Pt surface oxide.

S1 Component. This is the predominant S 2p component in spectra for all samples in our study (Figures 1, 5, and 7; Table 3) with the BE between 162.3 and 162.4 eV. On the basis of this BE, we assign the S1 component as alkylthiolates bound to the Pt substrate, in agreement with the reported S 2p BE values for alkylthiolates on other fcc metals: 161.9−162.1 eV on Au,[9,10,17,18,20−24,28,38,39,62] 161.8−162.3 eV on Ag,[9,23,28,62] 162.1−162.5 eV on Cu,[9,29,31] and 161.8 eV on Ni.[32]

An alternative assignment for S 2p components in this BE range was suggested in a recent study of SAMs on Pd: A 162.3 eV BE component was assigned as "sulfur present in a metal sulfide interphase", and a 163.2 eV BE component was assigned as alkylthiolates.[33] Such an assignment required C−S bond scission,[33] a process believed possible on catalytic metals. Given the striking similarity of the SAMs/Pd S 2p data to ours and the catalytic nature of Pt, we carefully examined the possibility of this alternative assignment for SAMs/Pt. We found three pieces of evidence that rule out such a possibility. First, the S1 component falls within the range observed for alkylthiolates on fcc metals, whereas the S2 component (163.2 eV) clearly does not.[63] Second, in all as-deposited monolayers on Pt, the S 2p doublet spin−orbit splitting of the S1 component is well-resolved, and its fwhm of 0.98 eV is only 17% larger than the 0.84 eV fwhm measured for the reference C6SH/Au monolayer.[16] The narrow width and absence of systematic trends in residuals indicate that it is a single spectral component, in contrast to a combination of a peak and a low-BE shoulder typically observed after C−S bond scission on fcc metals. Finally, the XPS stoichiometry data in section 4.1 indicate that there is no loss of C from as-deposited or solvent-treated monolayers and, hence, that no C−S bond scission occurs. This stoichiometry analysis rules out the putative mechanism required for the alternative assignment of S1.

S2 Component. There are several possible assignments for the S2 component at 163.2 eV BE.[7] Two interpretations that we rule out are radiation (or electron) damage[19,39,64] and unbound thiols.[10,17,18] On Pt, the radiation-damage interpretation appears unlikely, given that a recent study showed that the S2 component did not change after 10 h of irradiation by a Mg Kα source.[7] In our experiments designed to test the unbound thiol interpretation,[5,7] the intensity of the S2 component remained essentially unchanged (Figure 1 and Table 3) after extensive rinsing or overnight soaking in CH_2Cl_2, a good solvent that should significantly reduce an unbound component.[17] Concurring with these XPS results, our RAIRS data also did not show S−H vibrational modes expected for unbound thiols.

For S2, the consistent 0.9 eV BE shift, narrow fwhm, and insensitivity to deposition conditions suggest that it corresponds

(59) Lang, P.; Mekhalif, Z.; Rat, B.; Garnier, F. *J. Electroanal. Chem.* **1998**, *441*, 83−93.
(60) Toulhoat, H.; Raybaud, P.; Kasztelan, S.; Kresse, G.; Hafner, J. *Catal. Today* **1999**, *50*, 629−636.
(61) Polcik, M.; Wilde, L.; Haase, J.; Brena, B.; Comelli, G.; Paolucci, G. *Surf. Sci.* **1997**, *381*, L568-L572.
(62) Zharnikov, M.; Frey, S.; Heister, K.; Grunze, M. *Langmuir* **2000**, *16*, 2697−2705.
(63) The BE reported in ref 65 for S 2p in bulk PtS is 162.9 eV is closer to S2 rather than S1. Only for bulk PtS_2 is the BE comparable at 162.4 eV (ref 66), but creating a stoichiometry similar to PtS_2 at the surface would require C−S bond scission for the majority of alkylthiolates, i.e., such an assignment for S1 is incompatible with the rest of the data.
(64) Heister, K.; Zharnikov, M.; Grunze, M.; Johansson, L. S. O.; Ulman, A. *Langmuir* **2001**, *17*, 8−11.

to a specific binding geometry rather than simply a collection of random surface sites. Three possible interpretations are suggested by the literature and chemical intuition: sulfur headgroups bound to platinum oxide, alternative surface binding sites, or the presence of disulfides.

Support for the argument that the S2 component arises from sulfur functional groups bound to platinum oxide comes from a systematic study of SAMs on an oxidized Au surface,[21] which showed two S 2p components with BEs of 162.1 and 163.3 eV. The intensity of the 163.3 eV component was correlated with oxygen exposure for monolayers prepared in UHV, and it did not change after 4 h of irradiation by a Mg Kα source. Alkanethiols adsorb on gold oxide with higher density and lower tilt angle than on clean Au[21]—properties that closely parallel the results for SAMs on Pt. Additional evidence that the S2 component is related to platinum oxide is presented in ref 5. The S 2p spectrum is noticeably shifted for a C18SH monolayer on platinum oxide compared to that on clean Pt. Although individual S 2p components are not resolved in the spectrum shown in ref 5, the overall shift of the S 2p envelope appears to be at least 0.7−0.8 eV to higher BE, i.e., very close to the 0.9 eV shift of S2. The data in ref 5 confirm that alkanethiols can adsorb on platinum oxide and that the BE for a large fraction of such monolayers is consistent with S2. A possible binding geometry is to a Pt atom that has an O nearest neighbor and thus shares a smaller fraction of its electron density with the S compared to a regular Pt surface atom.[59] BE shifts reported for platinum oxide and bulk platinum sulfides are consistent with this binding geometry.[54,65,66] The only significant inconsistency of this interpretation is that, whereas the oxygen-free deposition on TS-Pt reduced[44] S2 and deposition on heavily oxidized Pt produced primarily S2,[5] deposition on slightly oxidized UVO-Pt did not affect S2. In other words, the positive correlation between S2 and the amount of surface oxide (such as observed for monolayers on oxidized Au[21]) is not strictly followed for monolayers on Pt. There is also no positive correlation between S2 and postdeposition oxidation in air (Figures 5 and 7).

The alternative binding site interpretation, i.e., the binding of sulfur to a Pt surface site different from that giving rise to the S1 component, has limited support from the available data for other fcc metals. On Au, no significant BE differences have been observed between Au(111) single crystals and various polycrystalline Au surfaces (including oxidized ones); however, oxidation dependence on the structure of polycrystalline Au films has been reported.[21,22,67] Whereas multiple binding sites and incommensurate monolayers have been reported on other fcc metals,[68−71] the typical S 2p BE differences are rather small—the largest reported value we found was ∼1 eV difference for S chemisorbed at different binding sites on Ni(111) vs Ni(001).[72,73] Therefore, S2 assignment to alternative binding sites would require that, on polycrystalline Pt, the energy difference between the sites be particularly high, in disagreement with existing data for methanethiol on Pt(111).[74] The strongest support for the alternative binding site interpretation in our data comes from the results for monolayers on TS-Pt, the only case where S2 was significantly reduced. TS-Pt is considerably smoother than polycrystalline Pt and thus potentially has fewer alternative binding sites.

The third potential interpretation for S2 is the formation of disulfide moieties when alkanethiols self-assemble on Pt. If disulfides exist on the Pt surface, it is possible that S−Pt bonding occurs through only one of the S atoms (S1), while the second S atom (S2) remains unattached to the surface. The major advantage of this interpretation is that the relative fraction of molecules adsorbed in disulfide form might depend on both surface oxidation and roughness. Disulfides might, in fact, form as a result of reducing surface oxides. One discrepancy in this model is the clearly missing S1 component in the data for monolayers on platinum oxide,[5] where an enhancement of the disulfide formation (and attachment) can be expected. Considering the disulfide interpretation of S2 underscores the inherent difficulty of definitively assigning such features—the debate about the adsorption of disulfides on gold surfaces has been going on for decades. Experimentally, it is extremely difficult to unambiguously determine the structure of surface species present at submonolayer coverages.

One might expect that studies on single-crystal surfaces could provide more definitive structural information. However, recent limited studies of alkanethiol adsorption on clean single-crystal Pt(111) surfaces in UHV suggest the absence of long-range ordering and a much more complicated adsorption process than for prototypical SAMs on Au or Ag.[75,76] Similarly, a recent STM study provided evidence of local $(\sqrt{3} \times \sqrt{3})R30°$ ordering for alkanethiols on single-crystal Pt(111), but also reported difficulties with imaging any long-range ordering.[49] The presence of a disordered component such as S2 could naturally account for these observations.

5. Conclusions

We studied the formation of alkanethiol SAMs on Pt surfaces as a function of substrate cleaning, solvents used for deposition and post-treatment, and alkyl chain length. We also examined the long-term stability of such SAMs in air and the corresponding evolution of the monolayer structure with exposure to air. We find that a standard deposition using p-Pt substrates and 1 mM ethanolic solutions of alkanethiols for 20 h produced monolayers of equal or better initial quality compared with other reported methods. As-deposited SAMs on Pt are dense and have a nearly upright chain orientation. There is no evidence for either weakly adhering species or C−S bond scission. These SAMs are stable against short-term (about a week) exposure to ambient air but oxidize and degrade significantly after about a month.

XPS spectra of the S 2p region indicate that these monolayers consist of at least three components. The major component, S1, is assigned to alkylthiolates typical for SAMs on other metals. A minor component, S3, is associated with thiols in intermediate oxidation states. The remaining component, S2, corresponds to approximately one-third of the S layer. Only control experiments on TS-Pt substrates under oxygen-free conditions eliminated S3 and reduced S2; these two minor components were largely unaffected by other changes in deposition conditions. We cannot

(65) Dembowski, J.; Marosi, L.; Essig, M. *Surf. Sci. Spectra* **1993**, *2*, 104−108.
(66) Dembowski, J.; Marosi, L.; Essig, M. *Surf. Sci. Spectra* **1993**, *2*, 133−137.
(67) Lee, M. T.; Hsueh, C. C.; Freund, M. S.; Ferguson, G. S. *Langmuir* **1998**, *14*, 6419−6423.
(68) Fisher, C. J.; Woodruff, D. P.; Jones, R. G.; Cowie, B. C. C.; Formoso, V. *Surf. Sci.* **2002**, *496*, 73−86.
(69) Kariapper, M. S.; Fisher, C.; Woodruff, D. P.; Cowie, B. C. C.; Jones, R. G. *J. Phys.: Condens. Matter* **2000**, *12*, 2153-2161.
(70) Jackson, G. J.; Woodruff, D. P.; Jones, R. G.; Singh, N. K.; Chan, A. S. Y.; Cowie, B. C. C.; Formoso, V. *Phys. Rev. Lett.* **2000**, *84*, 119−122.
(71) Kariapper, M. S.; Grom, G. F.; Jackson, G. J.; McConville, C. F.; Woodruff, D. P. *J. Phys.: Condens. Matter* **1998**, *10*, 8661−8670.
(72) Mullins, D. R.; Huntley, D. R.; Overbury, S. H. *Surf. Sci.* **1995**, *323*, L287-L292.
(73) Mullins, D. R.; Tang, T.; Chen, X.; Shneerson, V.; Saldin, D. K.; Tysoe, W. T. *Surf. Sci.* **1997**, *372*, 193−201.
(74) Lee, J. J.; Fisher, C. J.; Bittencourt, C.; Woodruff, D. P.; Chan, A. S. Y.; Jones, R. G. *Surf. Sci.* **2002**, *516*, 1−15.
(75) Sweeney, T. M. M.S. Thesis, University of New Orleans, New Orleans, LA, 2004
(76) Yang, M.; Laracuente, A. R.; Whitman, L. J. Unpublished results, 2005.

unambiguously assign the S2 component; however, we propose that it could be related to platinum oxide, alternative binding sites, or the presence of disulfide groups.

Whether SAMs on Pt are inherently multicomponent remains an open question that clearly requires further study on both single-crystal and practical thin-film substrates. The inclusion of XPS characterization will be crucial for any future studies of SAMs/Pt, as to date, it has been the only technique to directly detect the multicomponent S chemistry at the interface. The multicomponent nature of alkanethiol SAMs on Pt should also be carefully considered in the interpretation of molecular electronic behavior of these systems.

Acknowledgment. The authors thank Drs. K. G. Kreider and C. D. Zangmeister (NIST) for preparation of the TS-Pt substrates and oxygen-free deposition of monolayers on these substrates. D.Y.P. thanks Drs. L. A. Baker, T. D. Clark, and J. C. Sullivan (NRL) for helpful discussions of the surface chemistry and characterization of SAMs; Prof. M. Grunze (Heidelberg, Germany) for a discussion of multicomponent SAMs; and Drs. V. M. Bermudez (NRL), C. J. Powell (NIST), and C. van der Marel (Philips Research, The Netherlands) for detailed comments and careful review of the XPS quantification methodology. Work at NRL was supported by the Office of Naval Research and the Air Force Office of Scientific Research.

Appendix A1. Quantification of Monolayer Thickness and Stoichiometry

In the standard XPS formalism, photoelectrons are assumed to be exponentially attenuated by an overlayer. For SAMs, the validity of this approximation has been established in a previous study, which also reported the corresponding energy dependence of electron attenuation length (EAL),[25] which we used in calculations for Table 2. The uncertainty in the SAM density does not affect these EALs; varying the density by a factor of 2 above and below 0.96 g/cm^3 (HDPE) resulted in <5% changes in the EALs.[77]

To determine the monolayer thickness in this approach, the intensities of Pt 4f and 4d peaks are measured for a SAM and for a freshly sputtered clean Pt surface. Using the exponential attenuation model and EAL values discussed above, for each monolayer, the Pt 4f and 4d intensity attenuation is converted into a thickness.

Predicting elemental ratios measured by XPS involves separate calculations for S and C signals. In the ideal SAM structure, the S signal is attenuated by the full thickness of the monolayer (S* in Table 2). For C, in the ideal structure, atomic layers corresponding to the alkyl chains are uniformly spaced within the total monolayer thickness. The contributions from each atomic layer of C are added from top to bottom with increasing attenuation (C* in Table 2). For example, for an ideal C18SH monolayer of 2.4 nm thickness, the intensity of the S signal coming through the monolayer is attenuated to S* = 0.53 of its original strength. For C, the attenuated intensity from all 18 layers adds up to C* = 13.3, and the calculated ratio is C*/S* = 25.1.

Appendix A2. Quantification of Sulfur Coverage

In a well-formed SAM, a single layer of sulfur atoms is located at the S−metal interface. Au 4f, Pt 4f, and S 2p photoelectrons are nearly identically attenuated by the hydrocarbon overlayer, because the difference in kinetic energies is <6%. A simple ratio of S/metal XPS intensities is then essentially independent of the detailed overlayer structure. By normalizing to the intensity of the substrate XPS peak, such as that shown in Figure 1, we can directly compare the S 2p spectra for different monolayers and obtain absolute sulfur coverages, n_S, as

$$n_S = \left(\frac{I_S}{I_M}\frac{\sigma_M}{\sigma_S}\right)\left(\frac{T_M}{T_S}L_M^Q N_M\right) \quad (1)$$

The first term in eq 1 contains the experimental I_S/I_M intensity ratio adjusted by the ratio of respective Scofield coefficients σ,[36] which allows direct comparison of SAMs on different metals M (Pt and Au in our case) and thus is used to report relative elemental intensities in Figures 1, 2, and 5−7 and Tables 2 and 3. In a standard empirical approach, the second term can be considered as a conversion coefficient between the Scofield cross sections[36] and empirical sensitivity factors. Equation 1, however, is written in the form suggested by ref 78, where T is the analyzer transmission function, N_M is the bulk atomic density of the metal substrate, and L_M^Q is the electron attenuation length for quantitative analysis (QEAL).[77−79]

The system for which we can quantitatively validate eq 1 is the reference C6SH/p-Au in Figure 1a. The parameters are $T_{Au}/T_S = 2845/2931$, $N_{Au} = 5.892 \times 10^{22}$ cm^{-3}, and $L_{Au}^Q = 1.745$ nm, which gives the second term in eq 1 as 9.98×10^{15} cm^{-2}. The value of L_{Au}^Q is calculated using NIST SRD-82 software,[77−79] which implements the TPP-2M formula for calculating electron inelastic mean free paths (IMFPs) and related parameters such as EALs.[78,80−83] For the C6SH/p-Au spectrum in Figure 1a, the Scofield-adjusted S/Au intensity ratio is 0.0455, and the S coverage is 4.5×10^{14} cm^{-2}. It is significant that both the intensity ratio and the calculated absolute sulfur coverage are in excellent agreement with the values reported for an alkanethiol SAM/Au in ref 22 and, of course, with 4.6×10^{14} cm^{-2} coverage expected for a complete alkanethiol SAM/Au.[8]

In the absence of a similarly well-defined absolute reference for SAMs/Pt, we use eq 1 for S/Pt intensity ratios corrected by an empirical sensitivity factor to account for differences between Au and Pt substrates. These absolute S coverage values are listed in Table 3, and the "Au reference" label indicates that the Au data were used as an absolute coverage reference. The details are described in the Supporting Information.

Supporting Information Available: RAIRS data for SAMs/TS-Pt. Oxidation of SAMs/Pt exposed to air. p-Pt and UVO-Pt substrate refractive index. Sulfur coverage quantification and EALs for Pt substrates. This material is available free of charge via the Internet at http://pubs.acs.org.

LA050928A

(77) Powell, C. J.; Jablonski, A. *NIST Electron Effective-Attenuation-Length Database*, version 1.0 (SRD-82); U.S. Department of Commerce, National Institute of Standards and Technology: Gaithersburg, MD, 2001.

(78) Jablonski, A.; Powell, C. J. *Surf. Sci. Rep.* **2002**, *47*, 35−91.

(79) Petrovykh, D. Y.; Kimura-Suda, H.; Tarlov, M. J.; Whitman, L. J. *Langmuir* **2004**, *20*, 429−440.

(80) Tanuma, S.; Powell, C. J.; Penn, D. R. *Surf. Interface Anal.* **1994**, *21*, 165−176.

(81) Tanuma, S.; Shiratori, T.; Kimura, T.; Goto, K.; Ichimura, S.; Powell, C. J. *Surf. Interface Anal.* **2005**, *37*, 833−845.

(82) Powell, C. J.; Jablonski, A. *J. Phys. Chem. Ref. Data* **1999**, *28*, 19−62.

(83) Powell, C. J.; Jablonski, A. *J. Vac. Sci. Technol. A* **1999**, *17*, 1122−1126.

Supporting Information

Alkanethiols on Platinum: Multicomponent Self-Assembled Monolayers

Dmitri Y. Petrovykh,[*,†,‡] Hiromi Kimura-Suda,[§,∥] Aric Opdahl,[§,£,#] Lee J. Richter,[§] Michael J. Tarlov,[§] Lloyd J. Whitman[‡]

[†]*Physics Department, University of Maryland, College Park, MD 20742;* [‡]*Naval Research Laboratory, Washington, DC 20375;* [§]*National Institute of Standards and Technology, Gaithersburg, MD 20899;* [∥]*Current address: PerkinElmer Japan Co., Ltd., Yokohama, Japan;* [£]*National Research Council Postdoctoral Associate at NIST;* [#]*Current address: Department of Chemistry, University of Wisconsin, La Crosse, WI 54601*

*Author to whom correspondence should be addressed: Dmitri Y. Petrovykh, Code 6177, Naval Research Laboratory, Washington, DC 20375-5342; E-mail: dmitri.petrovykh@nrl.navy.mil

RAIRS data for SAMs/TS-Pt. The spectra for the monolayers on TS-Pt substrates are intermediate between those for p-Pt and UVO-Pt (Figure SI1, Table SI1). The linewidths for TS-Pt are comparable to p-Pt, but the chain tilt, as reflected in the relative intensities of the CH_2 and CH_3 features, is comparable to UVO-Pt.

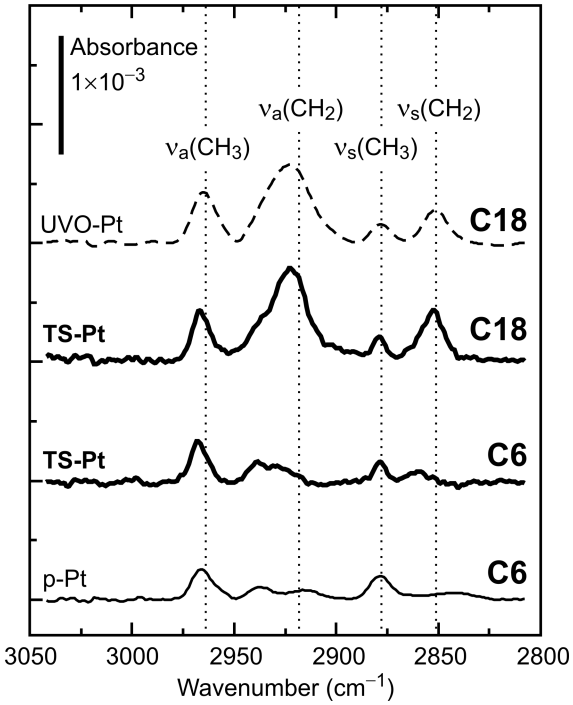

Figure SI1. RAIRS spectra of C-H region for C6SH and C18SH SAMs prepared on TS-Pt substrates compared to counterparts on p-Pt and UVO-Pt. Deposition from 1 mM ethanolic solutions, rinse in EtOH.

Table SI1. Vibrational Line Positions for C18SH/TS-Pt

Peak Assignment	ν, cm^{-1}	fwhm, cm^{-1}
$\nu_s(CH_2)$ sym str	2852	12
$\nu_s(CH_3)$ sym str	2879	6
$\nu_a(CH_2)$ asy str	2922	18
$\nu_s(CH_3)$ FR sym str	2939	12
$\nu_a(CH_3)$ op asy str	2966	8

Table SI2. Oxidation of SAMs/Pt Exposed to Air

Time in air	S 2p Components [a]				O 1s [a]
	S3	S2	S1	S 2p Total	
1.5 h					
C6	109	192	540	841	593
C12	99	147	531	777	637
C18	87	205	564	856	398
47 h					
C6	109	178	512	799	718
C18	70	152	555	777	505
5 days					
C6	129	174	491	794	1015
C12	206	158	426	790	1162
C18	95	143	428	666	1026
29 days[b]					
C12	452	74	263	789	2219
C18	318	92	289	699	1370

[a]Intensities for each element X are reported as Scofield-adjusted intensity ratios to Pt $4f_{7/2}$ substrate signal $(I_X/I_{Pt})(\sigma_{Pt}/\sigma_X)$ to enable direct comparison between S 2p and O 1s intensities.[36,37] In order to avoid multiple additional decimal characters, all the values are listed multiplied by a factor of 10^4.

[b]For the "29 days" samples, the three highest BE components (Figure 5, bottom) are included in the S3 intensity.

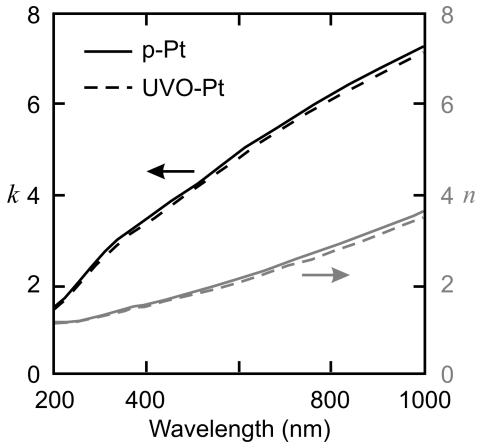

Figure SI2. P-Pt and UVO-Pt substrate refractive index. Real (n) and imaginary (k) parts of the Pt substrate refractive index $n + ik$ derived from the multiple sample SE analysis.

Sulfur Coverage Quantification and EALs for Pt Substrates

The standard XPS formalism used to calculate an absolute S coverage from an experimental I_S/I_M intensity ratio is described in the Appendix A2. The formalism used to derive eq 1 (Appendix A2) has been developed and examined over the last three decades and its reliability is generally accepted.[77-80] In Appendix A2, we validate this approach by the reference measurements of SAMs/Au, which agree with previously published results for both intensity ratios and absolute coverages.[22]

The direct application of eq 1 (Appendix A2) to experimental S/Pt intensity ratios however runs into unexpected complications. It is important to emphasize the distinction between the conversion of relative peak intensities into absolute coverage

values and the relative intensities themselves. The relative intensities in Figures 2, 7, and Tables 3, SI2 are obtained directly from the raw data, and thus are independent of the absolute quantification. Therefore, the conclusions from Sections 3 and 4 on monolayer thickness, stoichiometry, S 2p components, and relative coverage changes are not affected by any discrepancy in the absolute coverage quantification. As elaborated in the following, the unexpected failure of the quantitative EAL formalism in the Pt case defies simple explanations and thus represents a subject of a completely unrelated study, but fortunately we had enough reference data to identify and implement a practical solution in the form of an empirical sensitivity factor.

For S/Pt coverage eq 1 (Appendix A2) can be re-written as:

$$n_S = \left(\frac{I_S}{I_{Pt}}\frac{\sigma_{Pt}}{\sigma_S}\right)\left(\frac{T_{Pt}}{T_S}L^Q_{Pt}N_{Pt}\right) \quad (2)$$

Formal parameters analogous to the Au case in Appendix A2 are: T_{Pt}/T_S =2831/2931, N_{Pt}=6.622×10^{22} cm^{-3}, and L^Q_{Pt}=1.647 nm (L^Q_{Pt} calculated using NIST SRD-82 software[77-79]), which gives the second term in eq 2 as 10.53×10^{15} cm^{-2}. The first term in eq 2 suggests Scofield-adjusted S/Pt intensity ratios as a natural representation for the experimental intensity ratios.[36,37] A Scofield-adjusted intensity ratio of 0.0455 represents a unit of 1 in Figure 2 and Table 3, from eq 2 for Pt the corresponding coverage is 4.8×10^{14} cm^{-2} ("Pt reference" in Table SI3).

Inspection of the "Pt reference" absolute coverage values in Table SI3 reveals that they are physically impossible, even if packing with density of HDPE is assumed for the alkyl chains in the SAM. What is the source of this discrepancy?

The two numerical factors that could contribute to the coverage discrepancy are the S 2p/Pt 4f$_{7/2}$ intensity ratio itself and the estimate of the absolute number of Pt atoms contributing to the XPS signal (second term in eq 2). Another factor, albeit more difficult to quantify, is the structure (morphology) of the Pt substrate.

S 2p/Pt 4f$_{7/2}$ intensity ratio. For a fixed amount of S, the observed S 2p/Pt 4f$_{7/2}$ intensity ratio can be increased by S migration from the SAM/Pt interface to the top of the monolayer. There are four independent observations that rule out such a possibility in our case. First, the S1 component corresponds to alkylthiolates chemisorbed on Pt, thus only the S2 and S3 components can be associated with the hypothetical migrating molecules; for C18SH, the attenuation of the S signal by the monolayer is about 50% (Table 2), so even assuming that the entire S2 and S3 intensities represent S atoms on top of the monolayer is not sufficient to account for the observed S/Pt intensity ratio. Second, for molecules to migrate they must be weakly bound within the monolayer; the null result of the CH_2Cl_2 treatments argues against the presence of such weakly bound molecules. Third, any mechanism that artificially increases the S/Pt ratio must similarly affect the S/C ratio; it is extremely unlikely that any effect (e.g., adventitious carbon) could compensate for the hypothetical S enrichment for *all three* alkyl chain lengths in our study. Fourth, the thiol groups on migrating molecules must be subject to increased oxidation in the ambient; the data in Table SI2 and Figure 7 suggest that S1 rather than S2 and S3 is primarily oxidized during the first five days in air.

A sub-monolayer of oxide *between* the Pt substrate and the thiol groups can affect the measured S 2p/Pt 4f$_{7/2}$ ratio by attenuating the Pt signal. The total O 1s signal is less than the total S 2p signal for as-deposited monolayers (Table SI2 and Figure 7), therefore a full layer of Pt can be used to set a definite upper limit on attenuation of the substrate signal by the oxide, which corresponds to about 25%, i.e., again insufficient to account for the observed coverage discrepancy.

Table SI3. Sulfur Coverage for SAMs/Pt

Sample Description	Normalized S 2p Intensity[a]	Total Sulfur Coverage, 10^{14} atoms/cm^2	
		Pt reference[b]	Au reference[c]
p-Pt, EtOH			
C6SH	1.85	8.9	5.9
C12SH	1.71	8.2	5.5
C18SH	1.88	9.0	6.0
p-Pt, EtOH/CH_2Cl_2			
C6SH	1.70	8.2	5.5
C18SH	1.91	9.2	6.1
p-Pt, CH_2Cl_2			
C6SH	1.70	8.2	5.5
C18SH	1.94	9.3	6.2
UVO-Pt, EtOH/CH_2Cl_2			
C6SH	1.73	8.3	5.5
C12SH	1.82	8.7	5.8
C18SH	1.82	8.7	5.8
TS-Pt, EtOH, Ar			
C6SH	1.39	6.7	4.5
C18SH	1.52	7.3	4.9

[a]Intensities of S 2p components correspond to those in Figure 1 and are reported relative to the S 2p peak for C6SH/p-Au sample, i.e., as Scofield-adjusted[36,37] S 2p/Pt 4f$_{7/2}$ intensity ratios divided by 0.0455.

[b]From eq 2, one intensity unit used in the "Pt reference" column corresponds to the coverage of 4.8×10^{14} cm^{-2}.

[c]Absolute coverages calculated using a clean Au absolute reference and an empirical sensitivity factor to account for the difference between Pt and Au substrates (see text). Numerically, this corresponds to the "Pt reference" values divided by 1.5.

Pt reference. The absolute number of Pt atoms that contribute to the XPS signal is determined by the product ($N_{Pt}L^Q_{Pt}$) of the Pt atomic density N_{Pt} and the electron attenuation length (QEAL) within the Pt substrate L^Q_{Pt}. We used the standard value for Pt density. The actual density of the top layer (several nm thick) in polycrystalline Pt films clearly can differ from the tabulated bulk value, but by not more than a few percent, i.e., vastly insufficient to account for the observed coverage discrepancy.

The QEAL was calculated using NIST SRD-82 software.[77-79] The authors of the software estimated the combined uncertainty of these EAL calculations at about 20-25%. Moreover, both Pt and Au have been recently used in a systematic study of electron inelastic mean free paths (IMFPs), which found no significant discrepancies either between these two metals or between experimental data and model predictions.[81] Systematic differences between calculated and measured EALs, attributed to surface effects not included in the model, have been previously reported to be on the order of 10%.[82,83] In other words, the IMFP calculation in NIST SRD-82 is carried out using the same TPP-2M predictive formula[80] that has been independently tested in ref 81 for both Au and Pt, therefore the 50% discrepancy between XPS signals from Au and Pt that we observed in this work is not likely to be caused by systematic discrepancies in the underlying formalism. Perhaps the most significant difference between Au and Pt w. r. t. TPP-2M calculations is the much higher electron density near the Fermi level in Pt, which will increase inelastic

scattering in Pt due to a mechanism not explicitly included in the TPP-2M model.

Inelastically scattered photoelectrons do account for a larger fraction of the total intensity of Pt core level peaks compared to Au (most notable for the 4f peaks). Therefore, there is a larger uncertainty associated with properly accounting for the inelastic background intensities in fitting Pt peaks. This uncertainty could affect the measured intensity ratios of Au and Pt peaks; however, a comparison of Pt peak intensity values obtained from a range of fitting models and parameters suggests that this uncertainty is ≤30%.

An empirical check of the Pt reference is a comparison between the clean reference Au and Pt signals. If the formal parameters used in eqs. 1 and 2 for Au and Pt are correct, the fully-normalized Au/Pt ratio should be strictly unity (eq 3).

$$\left[\frac{I_{\mathrm{Au}}}{\sigma_{\mathrm{Au}} T_{\mathrm{Au}} L^{Q}_{\mathrm{Au}} N_{\mathrm{Au}}}\right] \Big/ \left[\frac{I_{\mathrm{Pt}}}{\sigma_{\mathrm{Pt}} T_{\mathrm{Pt}} L^{Q}_{\mathrm{Pt}} N_{\mathrm{Pt}}}\right] \equiv 1 \qquad (3)$$

In our experiments this normalized ratio is 1.51±0.06, thus clearly the quantitative description that works well for Au substrates, fails for Pt. Moreover, the ratio is identical for p-Pt and TS-Pt substrates, thus surface structure and roughness are largely ruled out as a factor, as these two types of substrates are dramatically different in terms of roughness (see Materials and Methods).

The above represents only a summary of our attempts to find a fundamental solution or explanation to this discrepancy—an extensive list of factors that we have considered is too long to be presented here, but we could not find a satisfactory solution. However, in practical terms the stability of the empirical Au/Pt reference intensity ratio suggested a very simple solution to the quantification problem—the factor of 1.5 can be used to correct the "Pt reference" values, effectively converting them to the "Au reference" validated by us and others (Tables 3, SI3). As already indicated, in formal terms this corresponds to introducing an empirical Au/Pt sensitivity factor—a procedure typically used when no internal standards or *a priori* parameter values are available.

REFERENCES

(1) Chen, Y.; Ohlberg, D. A. A.; Li, X. M.; Stewart, D. R.; Williams, R. S.; Jeppesen, J. O.; Nielsen, K. A.; Stoddart, J. F.; Olynick, D. L.; Anderson, E. *Appl. Phys. Lett.* **2003**, *82*, 1610-1612.
(2) Beebe, J. M.; Engelkes, V. B.; Miller, L. L.; Frisbie, C. D. *J. Am. Chem. Soc.* **2002**, *124*, 11268-11269.
(3) Graff, K. *Metal impurities in silicon device fabrication*; Springer-Verlag: Berlin, 1995; Vol. 24.
(4) Vilar, M. R.; Bouali, Y.; Kitakatsu, N.; Lang, P.; Michalitsch, R.; Garnier, F.; Dubot, P. *Thin Solid Films* **1998**, *329*, 236-240.
(5) Li, Z. Y.; Chang, S. C.; Williams, R. S. *Langmuir* **2003**, *19*, 6744-6749.
(6) Brito, R.; Tremont, R.; Feliciano, O.; Cabrera, C. R. *J. Electroanal. Chem.* **2003**, *540*, 53-59.
(7) Laiho, T.; Leiro, J. A.; Lukkari, J. *Appl. Surf. Sci.* **2003**, *212*, 525-529.
(8) Schlenoff, J. B.; Li, M.; Ly, H. *J. Am. Chem. Soc.* **1995**, *117*, 12528-12536.
(9) Laibinis, P. E.; Whitesides, G. M.; Allara, D. L.; Tao, Y. T.; Parikh, A. N.; Nuzzo, R. G. *J. Am. Chem. Soc.* **1991**, *113*, 7152-7167.
(10) Rieley, H.; Kendall, G. K.; Zemicael, F. W.; Smith, T. L.; Yang, S. H. *Langmuir* **1998**, *14*, 5147-5153.
(11) Schoenfisch, M. H.; Pemberton, J. E. *J. Am. Chem. Soc.* **1998**, *120*, 4502-4513.
(12) Blackstock, J. J.; Li, Z. Y.; Freeman, M. R.; Stewart, D. R. *Surf. Sci.* **2003**, *546*, 87-96.
(13) Seah, M. P.; Gilmore, L. S.; Beamson, G. *Surf. Interface Anal.* **1998**, *26*, 642-649.
(14) Powell, C. J. *Appl. Surf. Sci.* **1995**, *89*, 141-149.
(15) Hesse, R.; Chasse, T.; Szargan, R. *Fresenius J. Anal. Chem.* **1999**, *365*, 48-54.
(16) The total fwhm is the sum of Gaussian and Lorentzian contributions. The Lorentzian fwhm was 0.1 eV for C 1s and O 1s, and 0.25 eV for S 2p. For C 1s components C2 and C3, the total fwhm was fixed to that of C1 (1.2-1.3 eV). For S 2p components we used spin-orbit intensity ratio of 0.5 and energy splitting of 1.2 eV; the total fwhm was 0.98 eV for S1 and S2, 1.48 eV for S3.
(17) Castner, D. G.; Hinds, K.; Grainger, D. W. *Langmuir* **1996**, *12*, 5083-5086.
(18) Ishida, T.; Hara, M.; Kojima, I.; Tsuneda, S.; Nishida, N.; Sasabe, H.; Knoll, W. *Langmuir* **1998**, *14*, 2092-2096.
(19) Heister, K.; Frey, S.; Golzhauser, A.; Ulman, A.; Zharnikov, M. *J. Phys. Chem. B* **1999**, *103*, 11098-11104.
(20) Heister, K.; Allara, D. L.; Bahnck, K.; Frey, S.; Zharnikov, M.; Grunze, M. *Langmuir* **1999**, *15*, 5440-5443.
(21) Yan, C.; Golzhauser, A.; Grunze, M.; Woll, C. *Langmuir* **1999**, *15*, 2414-2419.
(22) Kawasaki, M.; Sato, T.; Tanaka, T.; Takao, K. *Langmuir* **2000**, *16*, 1719-1728.
(23) Heister, K.; Zharnikov, M.; Grunze, M.; Johansson, L. S. O. *J. Phys. Chem. B* **2001**, *105*, 4058-4061.
(24) Yang, Y. W.; Fan, L. J. *Langmuir* **2002**, *18*, 1157-1164.
(25) Laibinis, P. E.; Bain, C. D.; Whitesides, G. M. *J. Phys. Chem.* **1991**, *95*, 7017-7021.
(26) Hansen, H. S.; Tougaard, S.; Biebuyck, H. *J. Electron Spectrosc. Relat. Phenom.* **1992**, *58*, 141-158.
(27) Himmelhaus, M.; Gauss, I.; Buck, M.; Eisert, F.; Woll, C.; Grunze, M. *J. Electron Spectrosc. Relat. Phenom.* **1998**, *92*, 139-149.
(28) Ohgi, T.; Fujita, D.; Deng, W.; Dong, Z. C.; Nejoh, H. *Surf. Sci.* **2001**, *493*, 453-459.
(29) Laibinis, P. E.; Whitesides, G. M. *J. Am. Chem. Soc.* **1992**, *114*, 9022-9028.
(30) Ron, H.; Cohen, H.; Matlis, S.; Rappaport, M.; Rubinstein, I. *J. Phys. Chem. B* **1998**, *102*, 9861-9869.
(31) Sung, M. M.; Sung, K.; Kim, C. G.; Lee, S. S.; Kim, Y. *J. Phys. Chem. B* **2000**, *104*, 2273-2277.
(32) Mekhalif, Z.; Laffineur, F.; Couturier, N.; Delhalle, J. *Langmuir* **2003**, *19*, 637-645.
(33) Love, J. C.; Wolfe, D. B.; Haasch, R.; Chabinyc, M. L.; Paul, K. E.; Whitesides, G. M.; Nuzzo, R. G. *J. Am. Chem. Soc.* **2003**, *125*, 2597-2609.
(34) Brito, R.; Rodriguez, V. A.; Figueroa, J.; Cabrera, C. R. *J. Electroanal. Chem.* **2002**, *520*, 47-52.
(35) Long, Y. T.; Herrwerth, S.; Eck, W.; Grunze, M. *Phys. Chem. Chem. Phys.* **2002**, *4*, 522-526.
(36) Scofield, J. H. *J. Electron Spectrosc. Relat. Phenom.* **1976**, *8*, 129-137.
(37) Normalizing elemental XPS signals by the corresponding Scofield factors (ref 36) is a standard way to correct for element-dependent photoelectric cross-section - the major factor that determines element-specific XPS intensities. This normalization ignores any spatial distribution of the elements, but provides a practical way to compare elemental intensities, as such Scofield-adjusted intensity ratios often appear in quantitative XPS analysis models (see Appendix).
(38) Vericat, C.; Vela, M. E.; Andreasen, G.; Salvarezza, R. C.; Vazquez, L.; Martin-Gago, J. A. *Langmuir* **2001**, *17*, 4919-4924.
(39) Zerulla, D.; Chasse, T. *Langmuir* **1999**, *15*, 5285-5294.
(40) The Tougaard model with parameters established for SAMs/Au (ref 26) predicts intensities of inelastic backgrounds to be much lower than the observed high BE shoulders of S 2p peaks. The asymmetric S 2p peak shapes thus correspond to multiple S 2p components.
(41) The spectra were analyzed by nonlinear least-squares fitting to multiple Lorentzian lines except in the case of the UVO-Pt substrate, in which a Gaussian line shape was required.
(42) Parikh, A. N.; Allara, D. L. *J. Chem. Phys.* **1992**, *96*, 927-945.
(43) Shi, J.; Hong, B.; Parikh, A. N.; Collins, R. W.; Allara, D. L. *Chem. Phys. Lett.* **1995**, *246*, 90-94.
(44) The oxygen-free deposition on TS-Pt substrates resulted in the lowest overall O 1s signals in our study. For C6SH/TS-Pt the Scofield-adjusted intensity ratios (same units as in Table SI2) are 227 for C2+C3 components, 220 for O 1s, and 101 for S2. The total intensity of the oxidized C components is equal to the total O signal, thus the data are consistent with essentially no PtO_x on the surface, while S2 is still present.
(45) Each of the alkanethiol molecules contains two chemically distinct carbon atoms: one bound to the sulfur head group and one in the methyl group. The former is likely to have BE higher than the alkyl carbons of the main C1 peak. The C2/C1 intensity ratios in fits to our data (Figure 6), however, are about half of what would be expected for ideal SAMs of respective thicknesses. An additional component of the appropriate intensity and BE shift < 1 eV can be added without sacrificing the quality of the fits to account for the head group bound carbons. C2 and C3 components then must be interpreted as due to adventitious and/or solvent molecules. In the literature, assignment of C 1s components with BE shifts of 1.2-1.6 eV (C2) and 2.7-3.6 eV (C3) varies, e.g., refs 6,27.
(46) MacPhail, R. A.; Strauss, H. L.; Snyder, R. G.; Elliger, C. A. *J. Phys. Chem.* **1984**, *88*, 334-341.
(47) Snyder, R. G.; Strauss, H. L.; Elliger, C. A. *J. Phys. Chem.* **1982**, *86*, 5145-5150.
(48) Arnold, R.; Terfort, A.; Woll, C. *Langmuir* **2001**, *17*, 4980-4989.
(49) Yang, Y.-C.; Yen, Y.-P.; Yang, L.-Y. O.; Yau, S.-L.; Itaya, K. *Langmuir* **2004**, *20*, 10030-10037.

(50) Puglia, C.; Nilsson, A.; Hernnas, B.; Karis, O.; Bennich, P.; Martensson, N. *Surf. Sci.* **1995**, *342*, 119-133.
(51) Stipe, B. C.; Rezaei, M. A.; Ho, W. *J. Chem. Phys.* **1997**, *107*, 6443-6447.
(52)Saliba, N.; Tsai, Y. L.; Panja, C.; Koel, B. E. *Surf. Sci.* **1999**, *419*, 79-88.
(53) Gambardella, P.; Sljivancanin, Z.; Hammer, B.; Blanc, M.; Kuhnke, K.; Kern, K. *Phys. Rev. Lett.* **2001**, *8705*.
(54) Bancroft, G. M.; Adams, I.; Coatsworth, L. L.; Bennewitz, C. D.; Brown, J. D.; Westwood, W. D. *Anal. Chem.* **1975**, *47*, 586-588.
(55) Li, Z. Y.; Beck, P.; Ohlberg, D. A. A.; Stewart, D. R.; Williams, R. S. *Surf. Sci.* **2003**, *529*, 410-418.
(56) Uncertainties are 1 standard deviation averaged over 5 measurement series.
(57) The unique extraction of dielectric constants from ultrathin (≤ 10 nm) films is problematic as the film thickness and index become correlated. The correlation coefficient between thickness and the real part of the index (*n*) was ~0.93. However, the estimated parameters are considered unique as the statistical estimate of the fit uncertainties on thickness and *n*, accounting for the off-diagonal elements of the error matrix, are comparable (~50% smaller) to the reported uncertainties based on multiple data sets.
(58) Gottesfeld, S.; Maia, G.; Floriano, J. B.; Tremiliosi, G.; Ticianelli, E. A.; Gonzalez, E. R. *J. Electrochem. Soc.* **1991**, *138*, 3219-3224.
(59) Lang, P.; Mekhalif, Z.; Rat, B.; Garnier, F. *J. Electroanal. Chem.* **1998**, *441*, 83-93.
(60) Toulhoat, H.; Raybaud, P.; Kasztelan, S.; Kresse, G.; Hafner, J. *Catalysis Today* **1999**, *50*, 629-636.
(61) Polcik, M.; Wilde, L.; Haase, J.; Brena, B.; Comelli, G.; Paolucci, G. *Surf. Sci.* **1997**, *381*, L568-L572.
(62) Zharnikov, M.; Frey, S.; Heister, K.; Grunze, M. *Langmuir* **2000**, *16*, 2697-2705.
(63) BE reported in ref 65 for S 2p in bulk PtS is 162.9 eV is closer to S2 rather than S1. Only for bulk PtS_2, the BE is 162.4 eV (ref 66), but creating stoichiometry similar to PtS_2 at the surface would require C-S bond scission for the majority of alkylthiolates, i.e., such assignment for S1 is incompatible with the rest of the data.
(64) Heister, K.; Zharnikov, M.; Grunze, M.; Johansson, L. S. O.; Ulman, A. *Langmuir* **2001**, *17*, 8-11.
(65) Dembowski, J.; Marosi, L.; Essig, M. *Surf. Sci. Spectra* **1993**, *2*, 104-108.
(66) Dembowski, J.; Marosi, L.; Essig, M. *Surf. Sci. Spectra* **1993**, *2*, 133-137.
(67) Lee, M. T.; Hsueh, C. C.; Freund, M. S.; Ferguson, G. S. *Langmuir* **1998**, *14*, 6419-6423.
(68) Fisher, C. J.; Woodruff, D. P.; Jones, R. G.; Cowie, B. C. C.; Formoso, V. *Surf. Sci.* **2002**, *496*, 73-86.
(69) Kariapper, M. S.; Fisher, C.; Woodruff, D. P.; Cowie, B. C. C.; Jones, R. G. *J. Phys.: Condens. Matter* **2000**, *12*, 2153-2161.
(70) Jackson, G. J.; Woodruff, D. P.; Jones, R. G.; Singh, N. K.; Chan, A. S. Y.; Cowie, B. C. C.; Formoso, V. *Phys. Rev. Lett.* **2000**, *84*, 119-122.
(71) Kariapper, M. S.; Grom, G. F.; Jackson, G. J.; McConville, C. F.; Woodruff, D. P. *J. Phys.: Condens. Matter* **1998**, *10*, 8661-8670.
(72) Mullins, D. R.; Huntley, D. R.; Overbury, S. H. *Surf. Sci.* **1995**, *323*, L287-L292.
(73) Mullins, D. R.; Tang, T.; Chen, X.; Shneerson, V.; Saldin, D. K.; Tysoe, W. T. *Surf. Sci.* **1997**, *372*, 193-201.
(74) Lee, J. J.; Fisher, C. J.; Bittencourt, C.; Woodruff, D. P.; Chan, A. S. Y.; Jones, R. G. *Surf. Sci.* **2002**, *516*, 1-15.
(75) Sweeney, T. M. M.S. thesis, University of New Orleans, New Orleans, LA, 2004
(76) Yang, M.; Laracuente, A. R.; Whitman, L. J. **2005**, unpublished.
(77) Powell, C. J.; Jablonski, A. *NIST Electron Effective-Attenuation-Length Database, Version 1.0 (SRD-82)*; US Department of Commerce, National Institute of Standards and Technology: Gaithersburg, MD, 2001.
(78) Jablonski, A.; Powell, C. J. *Surf. Sci. Rep.* **2002**, *47*, 35-91.
(79) Petrovykh, D. Y.; Kimura-Suda, H.; Tarlov, M. J.; Whitman, L. J. *Langmuir* **2004**, *20*, 429-440.
(80) Tanuma, S.; Powell, C. J.; Penn, D. R. *Surf. Interface Anal.* **1994**, *21*, 165-176.
(81) Tanuma, S.; Shiratori, T.; Kimura, T.; Goto, K.; Ichimura, S.; Powell, C. J. *Surf. Interface Anal.* **2005**, *37*, 833-845.
(82) Powell, C. J.; Jablonski, A. *J. Phys. Chem. Ref. Data* **1999**, *28*, 19-62.
(83) Powell, C. J.; Jablonski, A. *J. Vac. Sci. Technol. A* **1999**, *17*, 1122-1126.